DISCLAIMER

This report was prepared as an account of work sponsored by an agency of the United States Government. Neither the United States Government nor any agency thereof, nor any of their employees, makes any warranty, express or implied, or assumes any legal liability or responsibility for the accuracy, completeness, or usefulness of any information, apparatus, product, or process disclosed, or represents that its use would not infringe privately owned rights. Reference herein to any specific commercial product, process, or service by trade name, trademark, manufacturer, or otherwise does not necessarily constitute or imply its endorsement, recommendation, or favoring by the United States Government or any agency thereof. The views and opinions of authors expressed herein do not necessarily state or reflect those of the United States Government or any agency thereof. Reference herein to any social initiative (including but not limited to Diversity, Equity, and Inclusion (DEI); Community Benefits Plans (CBP); Justice 40; etc.) is made by the Author independent of any current requirement by the United States Government and does not constitute or imply endorsement, recommendation, or support by the United States Government or any agency thereof.

Final Technical Report (FTR)

Federal Agency/ Organization Element:	DOE/Energy Efficiency and Renewable Energy (EERE) Hydrogen and Fuel Cell Technologies Office (HFTO)
Award Number:	DE-EE0009618
Project Title:	High Efficiency and Transient Air Systems for Affordable Load-Following Heavy Duty Truck Fuel Cells
Recipient Organization:	Eaton Corporation
Project Period:	Start: September 14th, 2022 End: June 30th, 2025
Principal Investigator (PI):	James McCarthy, Jr. Chief Engineer (248) 808-4082 JimMcCarthy@eaton.com
Business Contact (BC):	Nelson Laret Senior Manager, Government Contracts and Compliance (440) 523-5164 NelsonSLaret@eaton.com
Teaming Partners:	Ballard Power Systems National Renewable Energy Laboratory
Submitted:	Aug. 29th, 2025

Acknowledgement: This material is based upon work supported by the U.S. Department of Energy's Office of Energy Efficiency and Renewable Energy (EERE) Hydrogen & Fuel Cell Technologies Office (HFTO) under the Hydrogen and Fuel Cells R&D 2021 FOA DE-EE0009618 award number.

Executive Summary:

Hydrogen fuel cell powered vehicles are one of the potential paths to reducing vehicle emissions. An important subsystem of the hydrogen fuel cell system is an air handling system that provides the needed oxygen (in air) to react with hydrogen in the fuel cell stack for electric power generation. Today's systems use an electric motor to power an air compressor that supplies oxygen to the fuel cell stack. This process requires significant electrical power and is the largest parasitic power loss in hydrogen fuel cell vehicles. In addition to parasitic power loss, hydrogen fuel cell systems often have reliability issues associated with the air handling system. Reliability is of significant concern for heavy duty applications (especially long-haul applications). This project aims to improve both the electrical power consumption and reliability of hydrogen fuel cell air handling systems to meet the needs of heavy duty on-highway vehicle applications.

To achieve improved air handling system efficiency and reliability, Eaton proposes the use of their Twin Vortices (TVS) compressor and TVS expander mechanically coupled together, along with liquid spray humidification (water dosing), advanced motor and inverter technology, and a waste heat recovery recuperator. Combination of these elements create system level efficiency improvements through reduction in system flow restriction, waste energy recovery, and improvements in compressor performance.

Air handling system performance is optimized and validated with system simulation (low and high fidelity) as well as with physical testing. Initial low fidelity system simulations are used to optimize the component architecture (components selection and size). The compressor and expander were built using the optimized sizing results. Physical testing is used to verify modeling accuracy and a final high fidelity system simulation is used to gather the final reported key performance metrics (simulation correcting for operating conditions unattainable in test lab).

Final project results show a full load electrical power consumption of 37kW. However, project findings show a path for ~50% electrical power consumption improvement (~24kW full load power consumption). Liquid spray humidification tends to have significant cooling effects that counteracts the usefulness of waste heat recovery in the recuperator, therefore a production system would likely have either a recuperator or water dosing system. In addition to electrical power consumption improvements, Eaton's air handling system is shown to provide the required durability and reliability for use in on-highway heavy duty vehicles.

Preliminary cost and manufacturability are also assessed in the project. Most system components are already in production for other use cases, except for the advanced inverter technology that is an up-and-coming technology. Therefore, the proposed system has relatively low manufacturing capability risks. Preliminary system cost also meets the DOE target.

Table of Contents

Background:

Eaton's project proposal was inspired by work previously completed by Eaton in an 2012-2016 DOE funded project (DE-EE0005665). This project used Eaton's positive displacement TVS compressor and expander for fuel cell air handling. The compressor and expander were integrated with an electric motor. A fixed gear ratio was placed in between the expander and motor to slow the expander speed relative to the compressor speed. Some key investigation areas of this project were performance improvements from optimized expander inlet air angle relative to the rotors, plastic rotor development as a potential low-cost rotor manufacturing method, preliminary system studies as well as preliminary studies of water dosing into the compressor. Both the system study and water dosing study were left incomplete due to project timing constraints.
The Eaton team looked at the results from this 2012-2016 project and recognized potential areas of improvement for system efficiency through use of waste heat recovery (recuperator) and optimized rotor speeds (differential gearbox). The Eaton team also wanted to do a more in-depth analysis of the effects of liquid water dosing as well as the system performance of the integrated compressor and expander to provide independent control of mass flow rate and pressure. Learnings from the expander inlet angle study were used in the expander inlet design. Additionally, the limited system performance testing indicated that the compressor and expander were incorrectly sized, leading the Eaton team to perform a more detailed system sizing optimization in simulation prior to component design.

Project Objectives:

The objective of the project is to define a highly efficient and responsive air system for on-highway commercial vehicle fuel cells and to demonstrate critical aspects of the proposed system with proof-of-concept testing. Technologies that would contribute to system efficiency include the following:

- Positive-displacement TVS machines that extend range of efficient system operation and tolerate mixed flows (liquid and gas)
- Waste energy recovery via an expander and a recuperator
- Mechanical transmission of recovered waste energy
- An approach to humidity management that enhances compressor performance
- State-of-the-art motor and inverter technology

Compression of a mixed flow (water + air) is not an isentropic process. Thus, isentropic compressor and expander efficiencies listed in the FOA were used to calculate equivalent system performance in terms of net electrical power consumption. Use of net electrical power consumption allows for an apples-to-apples comparison of the system efficiency improvements compared to FOA targets. Table 1 shows the targets established during the pre-contract application phase of the project compared to the final results. The DOE targets were met for most of the key metrics for the final demonstration.

Table 1: Key Metrics Targets

Key Metric		DOE 2030 Target	Final Results
Motor + Motor Controller Efficiency	**100% Flow**	92%	93%
	50% Flow	92%	94%
	Idle	80%	83%
Compressor/Expander Isentropic Efficiency	**100% Flow**	75/70 %	66 / 62%
	50% Flow	80/80 %	70 / 57%
	Idle	62/60 %	63 / 0%
System Response Time		2 seconds	0.62 seconds
Durability		25,000 hours	Air system reliability 52% at 25,000 hours
Reliability		50,000 MBRC	Air system MBRC estimate 1.84M
Number of Startup Shutdown Cycles		50,000	See discussion in Task 2.
Noise at Idle		65 dB-A @ 1m	Between 63.6 and 67.2 dB-A.
System Cost		$3600	$3183
System Volume		0.25 L/kW	0.24 L/kW
System Weight		0.5 kg/kW	0.16 kg/kW
Turndown Ratio		20	43.2
System Efficiency Expressed as Air System Electrical Power Consumption for 300kW Fuel Cell:			
Electrical Power Consumption	**100% Flow**	27.9 kW	37 kW
	50% Flow	10.8 kW	9 kW
	Idle	0.32 kW	0.22 kW

Generally, the development approach was to optimize the system and component selections in simulation, to create a proof-of-concept (and potentially subscale) test system that demonstrates performance attributes that are of highest risk, and to qualify other risks in design studies proposing potential product implementations that likely satisfy application requirements. Below is a summary of project tasks executed during the project.

1 Optimize air system efficiency
- 1.1 Modeling and simulation
  - 1.1.1 Build System Model
  - 1.1.2 Calibrate model to test data
  - 1.1.3 Optimize component sizes and specs
  - 1.1.4 Design control system
  - 1.1.5 Evaluate stability and response
  - 1.1.6 Create component duty cycles
- 1.2 Asses risk/benefit, perf targets for water dosing system
- 1.3 Proof-of-concept prototype
  - 1.3.1 Build System
    - 1.3.1.1 Design
    - 1.3.1.2 Procure
    - 1.3.1.3 Fabricate
  - 1.3.2 Create test capability
    - 1.3.2.1 Define methods and procedures

1.3.2.2 Design equipment
1.3.2.3 Procure/fabricate equipment
1.3.3 Test
1.3.4 Results documentation
2 Improve roots machines to meet life requirement
2.1 Spec compressor bearings, seals, gears for life requirement
2.2 Spec expander bearings, seals, gears for life requirement
2.3 Estimate cost and manufacturability
3 Maximize geartrain efficiency
3.1 Design max efficiency tooth forms
3.2 Estimate cost and manufacturability
4 Optimize electric drive system
4.1 Create motor model for system sims using TARDEC results
4.2 Analyze and optimize component lives
4.3 Estimate cost and manufacturability
5 Maximize recuperator effectiveness with AM technology
5.1 Optimize heat transfer and flow performance
5.2 Size recuperator
5.3 Estimate cost and manufacturability
6 Estimate cost and manufacturability
7 Project management and planning

Table 2: Milestone Summary Table

Milestone Summary Table						
Task Number	**Task or Subtask (if applicable) Title**	**Milestone Type (Milestone, Go/No-Go Decision Point, End of Project Goal)**	**Milestone Description (Go/No-Go Decision Criteria)**	**Milestone Verification Process (What, How, Who, Where)**	**Anticipated Date (Months from Start of the Project)**	**Anticipated Quarter (QTR from Start of the Project)**
1.1	Modeling and simulation	Milestone	Optimized system defined	Electrical Power Consumption, System Response Time, Turndown Ratio predictions by model meet or exceed DOE 2030 targets.	9	3
1.2	Assess risk/benefit, perf targets for water dosing system	Milestone	Water doser assessment	Report submitted to DOE	6	2
2	Improve Roots machines to meet life requirement	Milestone	Optimized Roots machines defined	Design study report submitted to DOE	15	5
3	Maximize geartrain efficiency	Milestone	Optimized geartrain defined	Design study report submitted to DOE	15	5
4	Optimize electric drive system	Milestone	Optimized electric drive system defined	Design study report submitted to DOE	12	4
5	Maximize recuperator effectiveness with AM technology	Milestone	Optimized recuperator defined	Design study report submitted to DOE	12	4

		Go/NoGo Decision Point 1	Electrical Power Consumption < 27.9 kW (@100% flow) 10.8 kW (50% flow) and 0.32 kW (@idle); System Response Time < 2s Turndown Ratio >20 Roots product test data < 65 dB-A @ 1m Component life/cost assessments establish path to DOE targets.	System performance predictions by simulation; Design study results	15	5
1.3.1	Build system	Milestone	Proof-of-concept prototype complete	In person (or via remote audio/video if necessary) demonstration of prototype system and summary report	19	7
1.3	Proof-of-concept prototype	End of Project Goal	Proof-of-concept testing complete and demonstrated	Test report submitted to DOE (in process)	27	9

Project Results and Discussion:

Task 1 Optimize air system efficiency:

Subtask 1.1: Modeling and Simulation:

NREL developed a two-phase modeling approach for system optimization, each with different fidelity levels. The Static Model, also known as the low fidelity model, simulated steady-state conditions with reduced fidelity for fast computation, enabling rapid evaluation of 55,080 design options. Results were post-processed for feasibility and ranked by efficiency. Optimized designs were then refined using the Dynamic Model, also known as the high fidelity model, which included fluid and mechanical dynamics to support control system development, assess stability, predict performance more accurately, and simulate dynamic loading. The Dynamic model was used to evaluate Key Metrics under conditions not easily replicated in testing, such as inclusion of the fuel cell, since testing was performed only on the air system.

The team identified a need to reinterpret DOE FOA air system data to represent system power consumption target. Fuel cell stack inlet conditions (mass flow, pressure, temperature, humidity) were chosen as the air system's power consumption performance benchmark. Since these were not specified in the FOA, they were derived using the Million Mile Fuel Cell Truck (M2FCT) Consortium's air system architecture and FOA compressor data. Simulations used these inlet conditions as control targets. Fuel cell stack downstream conditions were modeled using a Ballard stack, which may have caused expander inlet conditions to differ from FOA values.

Subtask 1.1.1: Build System Model:

Static (Low Fidelity) Model Methodology

The NREL Static Model, built in Python, included component modeling and system integration. Ballard provided fuel cell and humidifier data and Eaton supplied TVS machine performance maps, recuperator data, geartrain losses, motor specs, valve characteristics, and water dosing info. NREL used this data to create and test physics-based models for each component. NREL also created additional recuperator models for use in the optimization study. Components were implemented as modular Python classes to simplify debugging and feature updates. Where available, models were validated against experimental data. Figure 1 shows the modeled air system components.

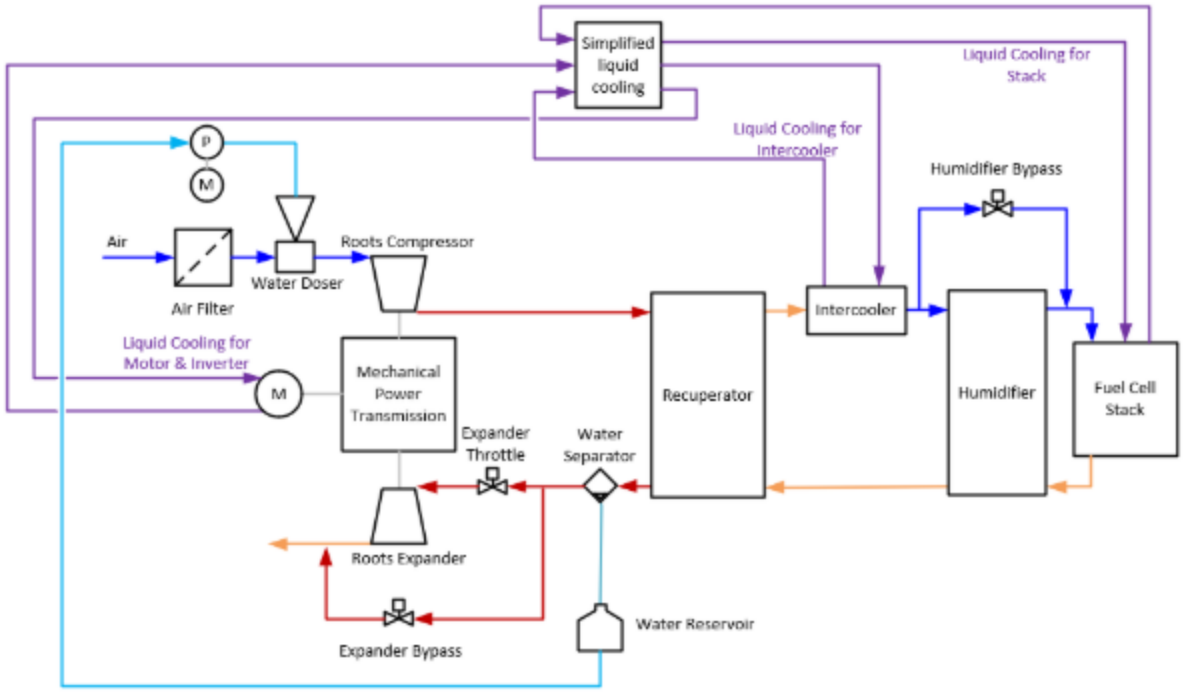

Figure 1: Proposed air system architecture

Static Model Component Descriptions

Fuel Cell Stack

The stack model was a look-up table based on data provided by Ballard. The Ballard datasets were generated using a pre-existing internal Ballard fuel cell stack model for HD applications. The datasets provide stack performance and outlet conditions.

TVS Machines (Compressor and Expander)

NREL used Eaton's analytically derived TVS machine performance maps to model compressors (R1000HPR, R1320HPR, R1650HPR) and expanders (V400, V500, V600) in the Static Model. Each was extrapolated ±10% in mass flow and displacement to cover a larger range of displacements. Using mass and energy balances, NREL calculated work output and compressor exit conditions. A wet compression model was developed to account for water dosing effects. Analytically derived performance maps

were compared to test data. Compressor models aligned well with shaft power and outlet temperature, but not volumetric efficiency. Expander models showed good correlation for shaft power and outlet temperature; volumetric efficiency couldn't be evaluated at the time of static model development.

Psychrometrics and Thermodynamics

To ensure the air handling system is providing proper humidification levels for efficient/reliable fuel cell stack performance, air humidity was calculated throughout the entire air system. The water state function calculations in the system simulation were implemented using the CoolProp library in Python. CoolProp contained psychrometric routines which were extensively validated against published ASHRAE (American Society of Heating, Refrigerating, and Air-Conditioning Engineers) references.

Motor and Inverter

The motor and inverter were modeled as a combined efficiency map linking shaft and electrical power. Thirteen maps of different continuous power ratings were created to support all system configurations (see Subtask 4.1 for map estimation process). Liquid cooling was assumed for both components, therefore FOA's 8% air flow allocation for motor cooling was excluded. To account for added liquid cooling demand, a parallel flow circuit was added. Based on Ballard data, the extra pump load was estimated as 3% of motor/inverter power losses and included in the system's net power consumption calculation.

Mechanical Power Transmission

The Static Model analyzed three mechanical power transmission setups: a single shaft, a differential gearbox, and two separate motors to connect the compressor and expander. Each configuration was individually modeled as follows.

Differential Geartrain

The differential geartrain was modeled as a planetary system with all three elements (ring, sun, carrier) in motion, assuming static equilibrium due to constant speed operation. Each air system component (compressor, expander, motor) was paired with each gear element, yielding six configurations per gear ratio across 11 ratios (1.4–4.5), totaling 66 combinations.

Compressor torque and speed were derived from performance maps based on outlet pressure and mass flow. Expander torque was calculated using:

$$\tau_r = \tau_s \frac{N_r}{N_s} = -\tau_c \frac{N_r}{N_r - N_s}$$

Expander pressure ratio and speed were then determined from map data. Motor speed was calculated using:

$$N_s\omega_s + N_r\omega_r - (N_s - N_r)\omega_c = 0$$

Eaton developed a geartrain loss model using SMT MASTA, assigning torque- and speed-dependent losses to each rotating element (e.g., bearings, seals, windage, gear meshes). Example loss equations below:

$$\eta_s = C_1 {\tau_s}^{C_2}$$

$$\widehat{P_s} = C_3 {\omega_s}^{C_4}$$

$$\eta_{sp} = C_5 \left(\omega_s - \omega_p\right)^{C_6}$$

For an example case where the expander was connected to the sun, the compressor was connected to the carrier, and the motor was connected to the ring, the total motor power is calculated as:

$$P_{motor} = \frac{\frac{\frac{-P_{comp} + \widehat{P_l}}{\eta_l} + \widehat{P_c}}{\eta_c} + \widehat{P_c}}{\eta_p} - \left(P_{exp}\eta_s - \widehat{P_s}\right)\eta_{sp}}{\eta_{rp}} + \widehat{P_r}}{\eta_r}$$

Single shaft

In single-shaft architectures, the compressor, expander, and motor share one shaft, forcing equal rotational speeds. Throttle and bypass valves are essential to maintain target stack inlet pressure. System viability with these valves is illustrated in the graphic

below.

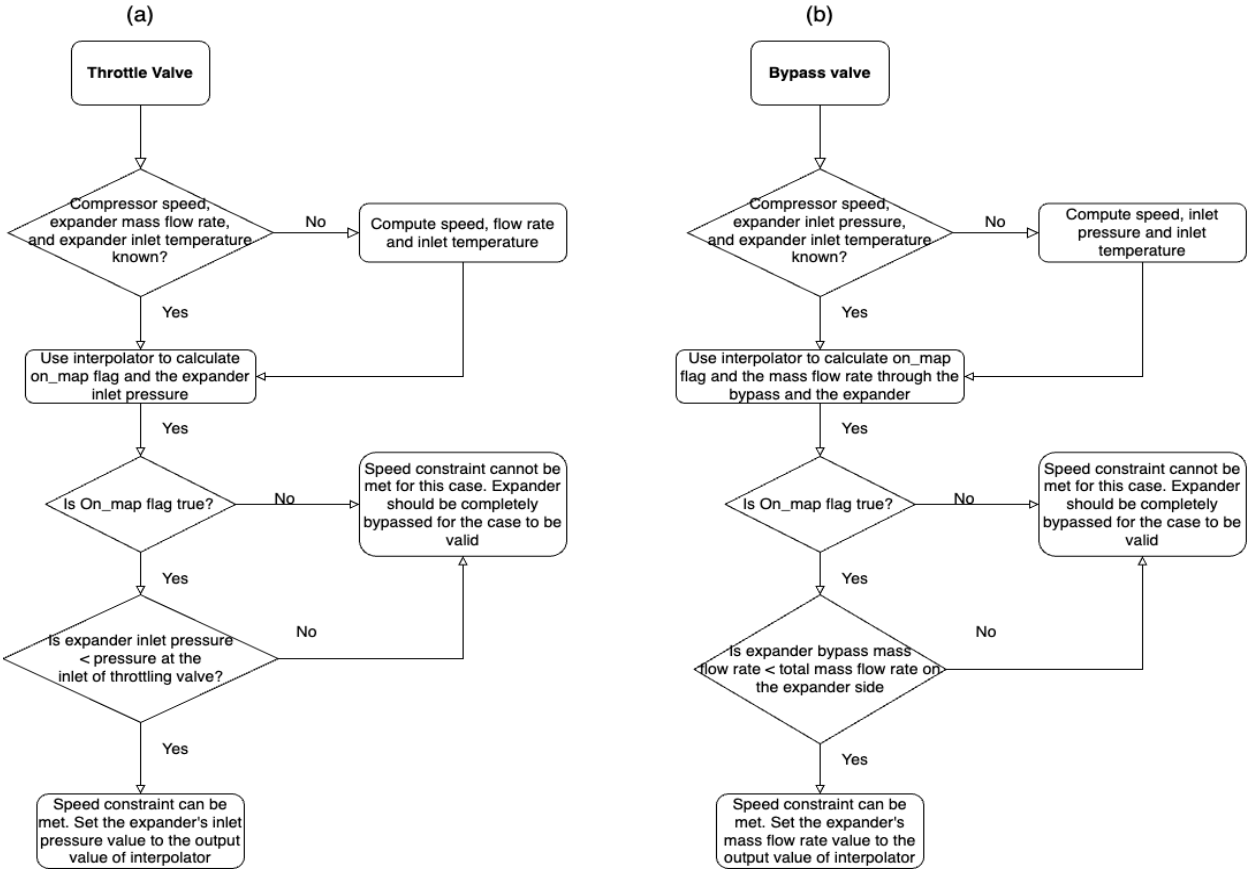

Figure 2: Throttle/bypass valve system viability logic

Crossflow Recuperator

Modeled using a lookup table based on Eaton's CFD and design tool data, the crossflow recuperator used six inputs (mass flow, temperature, pressure for each path) and three outputs (pressure drops and heat transfer). Eaton defined the geometry (see Task 5). NREL model used polynomial fits from table data to compute pressure drop and effectiveness.

Counterflow Recuperator

NREL modeled three counterflow designs (low, average, high effectiveness) using air-to-air stacked plate assumptions. Effectiveness was calculated via the NTU method using public plate heat exchanger data. Pressure drop was estimated using the Darcy-Weisbach equation.

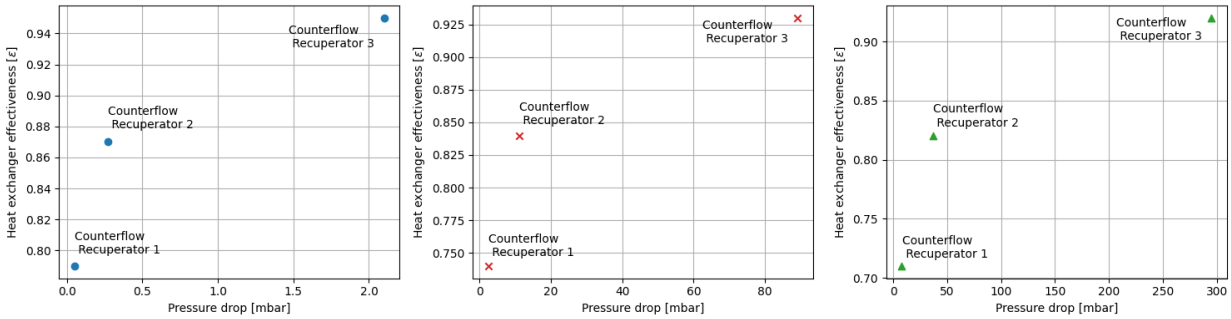

Figure 3: Static model recuperator performance

Humidifier

To evaluate architectures without water dosing, NREL developed a humidifier model using component data provided by Ballard. The model calculates water and heat transfer rates based on mass and heat transfer principles. A bypass valve enabled control of dry stream humidity and stack inlet conditions.

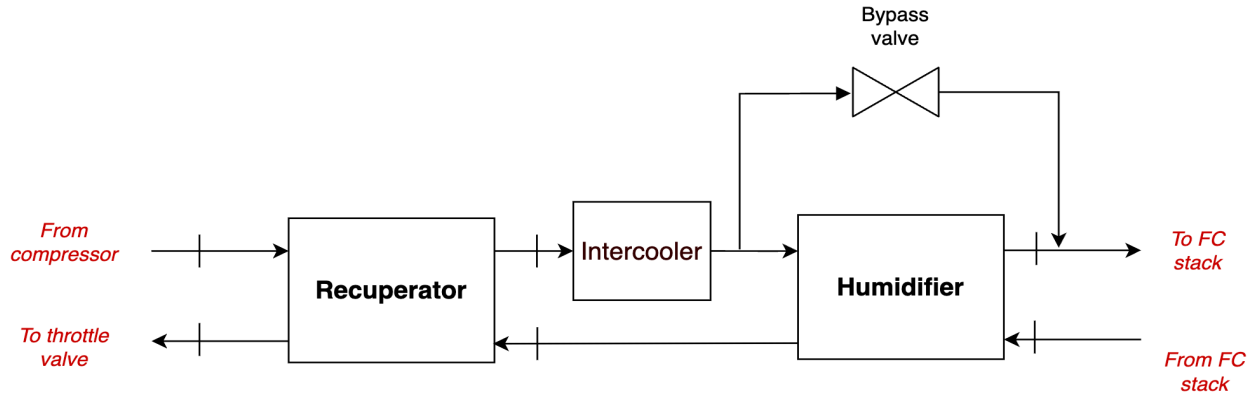

Figure 4: Schematic of humidifier integration into the system and humidifier control.

Using Ballard's operating data, the model determined the number of humidifier units needed, mass transfer efficiency, bypass mass ratio, wet outlet humidity, and pressure drop. Heat transfer was modeled using the NTU effectiveness method, accounting for psychrometry and liquid water evaporation.

Intercooler

The Static Model included an intercooler to maintain exact air temperature at 75°C before entering the fuel cell. Assumption was made that coolant suppling intercooler could come from either the radiator or fuel cell stack. Intercooler typically cooled air heated by compression using 70°C coolant from the radiator, but could also heat air using 80°C coolant from the fuel cell stack (for cases with water dosing). Coolant flow rate was assumed controllable to meet heat transfer needs.

Intercooler placement depended on system architecture:

- With humidifier: placed upstream to cool the dry stream below humidifier limits.
- With water dosing: placed between the recuperator and fuel cell stack.

Heating or cooling load was calculated from known inlet/outlet conditions upstream and downstream of the intercooler. Using data provided by Ballard, coolant pump load of 3% of heat transfer rate for cooling was assumed (zero load for heating).

Throttle and Bypass Valves

System simulations showed a valve was needed for independent pressure and mass flow rate control. Depending on architecture, valve was modeled either as a series throttle or a parallel bypass. NREL developed separate valve models using data provided by Eaton. Throttle valve had low flow resistance when open, while the bypass offered finer control at low angles. Valve behavior was defined by discharge coefficients varying with opening angle.

Fluid Conveyances

Fluid conveyance effects were not considered in the NREL Static Model. The pressure drops and thermal losses in the connecting pipes were considered negligible as compared to pressure drop in the components.

Air Filter

Air filter was modeled as a pressure drop on the air flowing from ambient air to the compressor inlet. Data for pressure drop as a function of air flow rate was provided by Eaton for a commercial vehicle engine air filter rated at 450 CFM airflow. Information was unavailable for air filters designed specifically for fuel cells rated for this airflow at the time of static model development.

Water Separator

The modeled water separator removed liquid water from the air stream for use in compressor water dosing. The water separator was located upstream of the expander and was modelled with 85% separation efficiency. Pressure drop across the water separator was calculated as a function of mass flow rate using data from a manufacturer.

Dynamic (High Fidelity) model methodology

The Dynamic Model builds on the Static Model by adding transient thermal-fluid behavior across air system components connected via piping. It includes three main solvers:

1. Pressure Solver
   Uses mass balance and the Hagen-Poiseuille equation to compute pressure changes across control volumes.
2. Thermal Solver
   Assumes wall thermal dynamics dominate air thermal dynamics and fluid volumes behave as well-stirred reactors. It calculates heat transfer between air, pipe walls, and ambient air using energy balance equations.
3. Humidity Solver
   Tracks water mass (liquid and vapor) and humidity along the air path. It accounts for evaporation (from water dosing) and condensation. Relative humidity and liquid water fraction are computed to ensure no condensation downstream of the compressor.

Each solver is tightly coupled, especially humidity and thermal solvers, due to the interdependence of temperature and moisture content.

A detailed explanation of the calculations performed in the static and dynamic models can be found in NREL's paper "Numerical and Experimental Investigation of a Novel Fuel-Cell Air-Handling System for Medium-Duty/Heavy-Duty Applications".

Subtask 1.1.2: Calibrate model to test data:

Static model

At the time of the static model development, limited test data was available for use in model calibration. As an alternative, the model outputs of each air system component were verified against the supplied data to the model. The verification approach for each component is shown in Table 3.

Table 3: Component verification approach summary

Component	Verification Process
TVS Machines (Compressor and Expander)	Model power result was compared to power data from TVS machine maps provided by Eaton for hundreds of operating points and a variety of displacements.
Recuperator	Thermal efficiency and pressure drop results from the Static Model were verified against the analytical model for counterflow recuperator designs.
Air Filter	Pressure drop results from the model were verified against pressure drop data from a commercially available air filter at a variety of mass flow rates.
Water Separator	Pressure drop results from the model were verified against the pressure drop data from the commercially available water separator for a variety of volumetric flow rates.
Throttle Valve	Since throttling is an isenthalpic process, enthalpy values at the inlet and outlet of throttle valve were used as the verification metric.
Humidifier	Mass balance (both liquid water and air) and energy balance constraints were verified. Pressure drop results from the model were checked against the pressure drop data provided by Ballard for their humidifier system.
Differential Geartrain	Gear speed and torque results from the model satisfied kinematic and static equations for a planetary gearset. Geartrain efficiency maps were reviewed with Eaton SMEs to verify that trends and magnitudes were consistent with expectations.

Dynamic model

Unlike the static model, test data was available for use in the dynamic model calibration/verification. Fluid conveyance geometries, and updated performance data of each system component was input into the dynamic model to be able to perform a direct comparison of model outputs to test data. Three step changes from rest were used to calibrate the model. The three target flow conditions are shown below.

Table 4: Model calibration flow conditions

	Stack Inlet Pressure (Bar Abs)	Mass Flow Rate [g/s]
50% Operating Point	1.6	131
100% Operating Point (Low Pressure)	2.3	262
100% Operating Point (High Pressure)	2.5	262

Test data was used as input into the Test System model, using directly measured compressor speed and pressure control valve position. The model's pressure, motor shaft power, and mass flow rate outputs were compared to measured data. Correlation was deemed acceptable if simulated pressure and mass flow rate were within ±10% of measured values. If not, modeling errors were investigated and corrected through iterative simulation and refinement. As shown in the graphs below, the model correlates well with mass flow rate, compressor outlet air temperature, and motor shaft power. Pressure response was acceptable but struggled to capture abrupt speed step changes at the expander inlet.

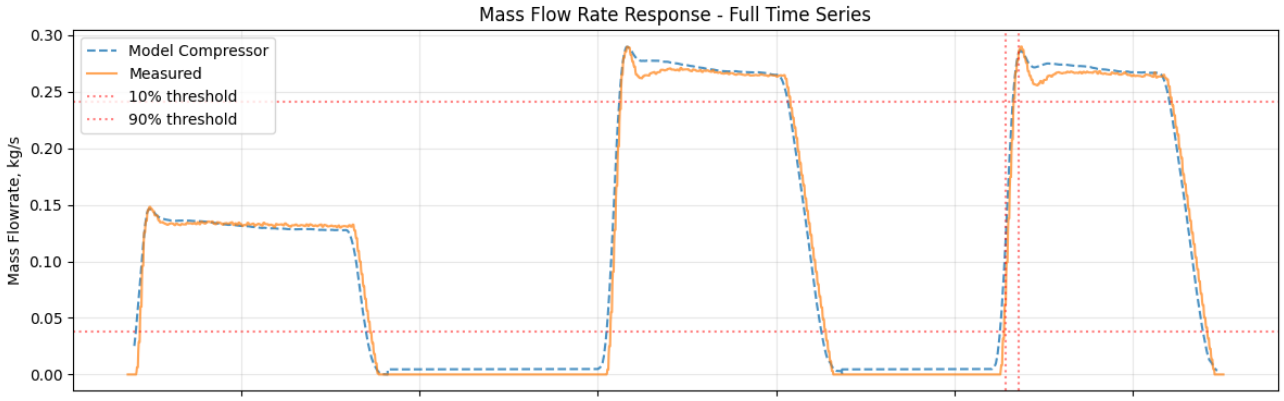

Figure 5: Mass flow rate correlation results

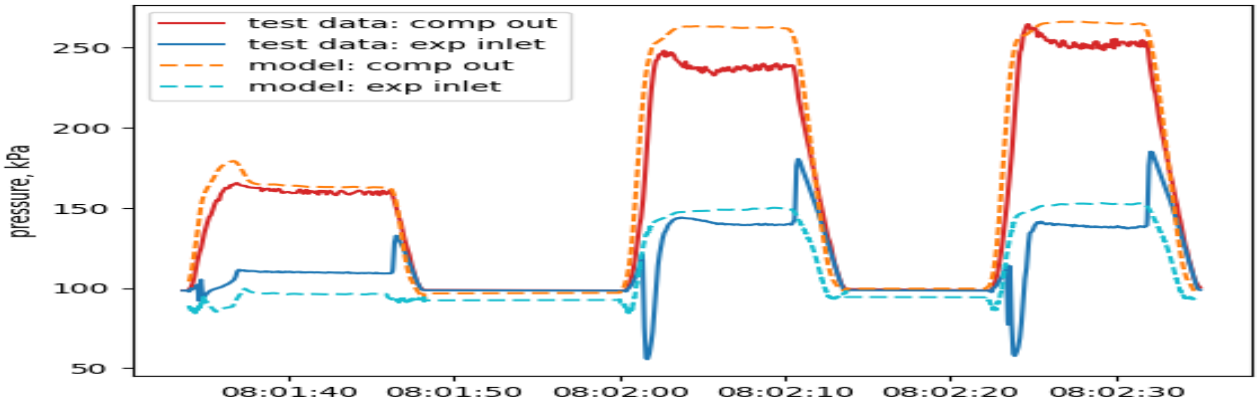

Figure 6: Pressure correlation results

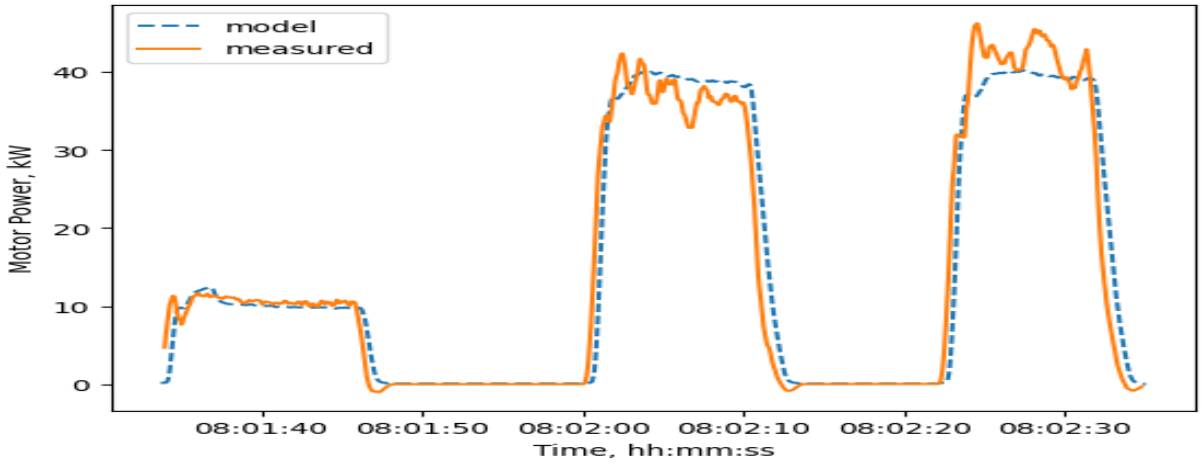

Figure 7: Shaft power correlation results

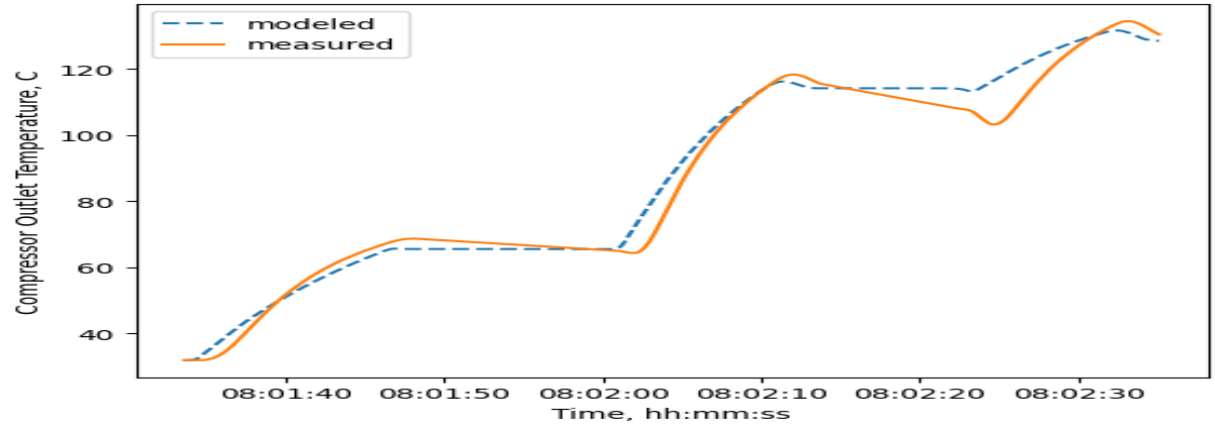

Figure 8: Compressor outlet temperature correlation results

Subtask 1.1.3: Optimize component sizes and specs:

Component sizing and system architecture optimization were performed using the NREL Static Model. Of the 55,080 architectures analyzed, undesirable cases were filtered out based on the following criteria:

1. Compressor operated outside its defined map at FOA 50% or 100% points.
2. Compressor or expander exceeded 14,000 RPM at any operating point.

Criterion 1 ensured reliable simulation within feasible machine operating ranges, excluding the Idle point due to instrumentation limitations providing poorly quantified data. Criteria 2 addressed durability concerns, as sustained operation above 14,000 RPM could accelerate bearing wear, preventing 25,000 hour durability.

Remaining cases were ranked by duty cycle weighted power, an average of net electrical power across three operating points, weighted by M2FCT duty cycle:

- 100% Point (70–100% stack power): 17.8% of M2FCT duty cycle
- 50% Point (30–70% stack power): 28.0% of M2FCT duty cycle

- Idle Point (10–30% stack power): 54.2% of M2FCT duty cycle

The top 20 cases showed a 7% spread in power consumption, with only 2% among the top 5. The optimized system identified below minimized air system electrical power consumption.

Mechanical Power Transmission: Single shaft
Compressor: R1188HPR
Expander: V550
Motor: 39kW and 34Nm continuous, 14,000rpm
Stack Pressure Control: Expander throttle and bypass valves
Stack Humidity Control: Water dosing at compressor
Recuperator: <20mbar pressure drop / ~75% effectiveness
Intercooler: Present
Duty Cycle Weighted Average Power: 7.8kW

Subtask 1.1.4: Design Control System:

Eaton had no prior controls experience for a coupled compressor-expander unit, making this a first-of-its-kind development. To reduce risk of component failure during controls design, a GT-Power plant model and a Simulink control model were created. Using GT-Power's co-simulation capability, the control logic was tested virtually and refined until performance was acceptable. The finalized control model was then implemented on the test stand for verification and tuning.

The controller manages:

- Mass flow rate via compressor speed
- Pressure via throttle and bypass valves positions
- Humidity via water dosing flow rate
- Temperature via intercooler coolant flow

Supporting software was also developed in Simulink to translate control model outputs into machine code for auxiliary systems (valve controller, motor drives, safety system) using Speedgoat hardware. This model also included safety logic to shut down the test stand in case of unit failure or runaway conditions.

Subtask 1.1.5: Evaluate stability and response:

Initial stability analysis using Eaton's GT model showed no issues with the single-shaft architecture. Instability was only observed in differential gearbox architectures when component loads couldn't balance, especially during startup due to unconstrained compressor and expander motion. Some instability could be mitigated by adjusting component layout and differential ratios. However, GT model limitations prevented deeper investigation. Instability with the differential was a contributing factor when deciding to pursue a single shaft architecture.

A preliminary response time estimate, from Eaton's GT model, for the single-shaft system with a 38kW motor showed 10–90% response times of 0.4 seconds for both

mass flow and pressure. Fast response was attributed to the motor's 34Nm torque and low system inertia, modeled as the sum of motor, compressor, and expander inertias.

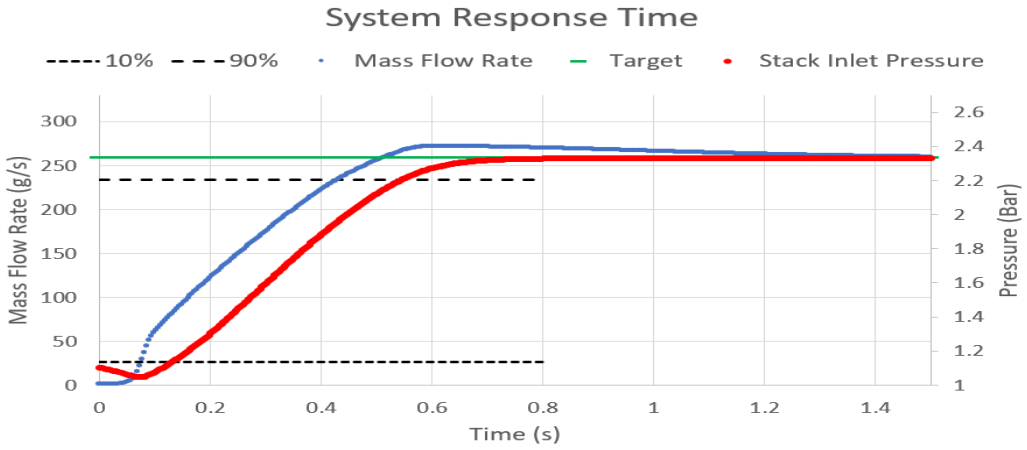

Figure 9: Preliminary system response time estimate

Response time results were validated with physical testing. With compressor torque limited to 34Nm, a 0–90% response time of ~0.62 seconds was measured with the recuperator installed and no water dosing. Water dosing had minimal impact due to it responding slower than the air system. Without recuperator, mass flow response slowed slightly (~0.64s), while pressure response improved. Dynamic model showed response of ~0.62s.

Two key factors influence response time:

- System air volume – Larger volumes slightly improves flow response but delays pressure response.
- Motor torque – Higher torque improves shaft acceleration, directly enhancing mass flow response.

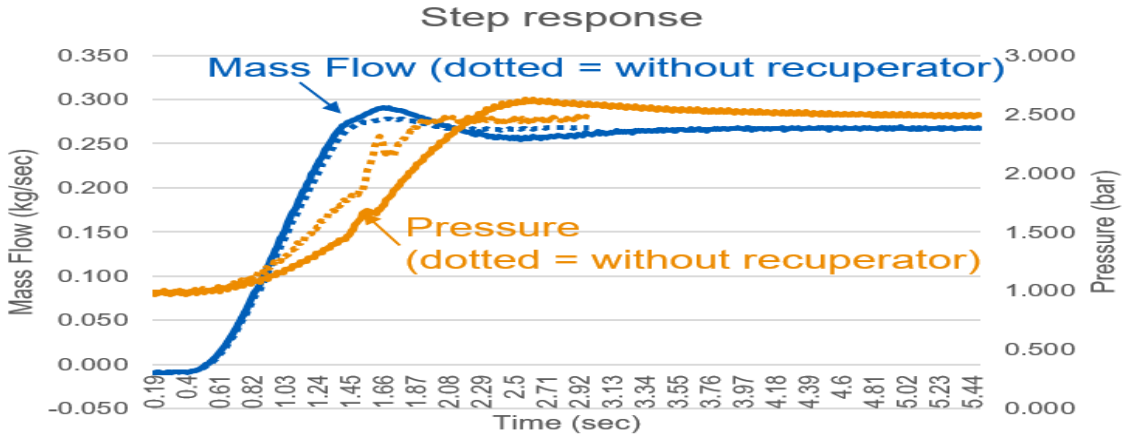

Figure 10: Tested system response time

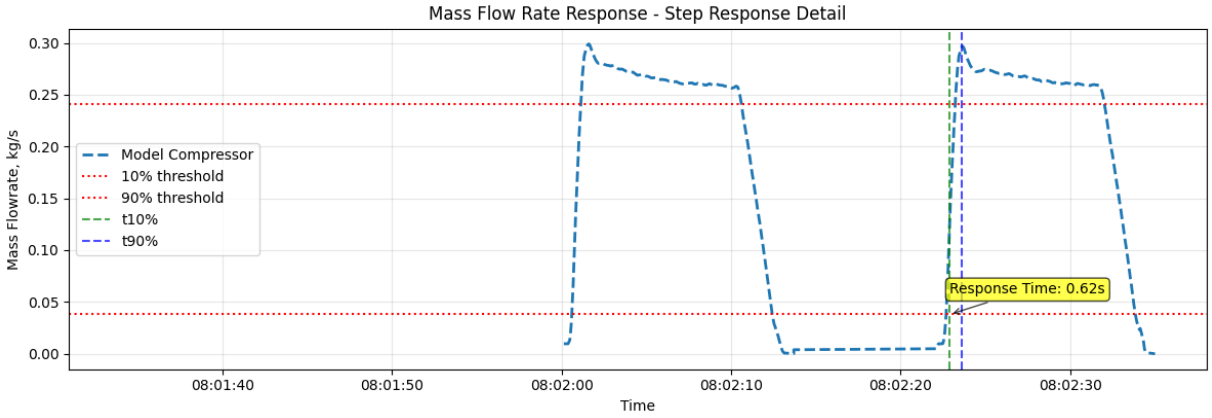

Figure 11: Dynamic model system response time results

Subtask 1.1.6: Create component duty cycles:

M2FCT provided a duty cycle for a 275kW load-following fuel cell system, detailing stack inlet pressure, mass flow, and power output. Stack outlet conditions were estimated using a regression model based on Ballard data normalized to 300kW. These inlet/outlet conditions were used in the NREL Static Model to generate duty cycles for the compressor, expander, motor, and power transmission.

The duty cycle showed sustained and rapid transients potentially expected for load following on-highway fuel cell applications. Rapid transient events could impact component life. Static Model does not account for inertial effects from acceleration. More realistic duty cycles, including dynamic loading, would require the NREL Dynamic Model, which was not used due to project timing constraints. A detailed component duty cycle analysis would be completed before any future product launch.

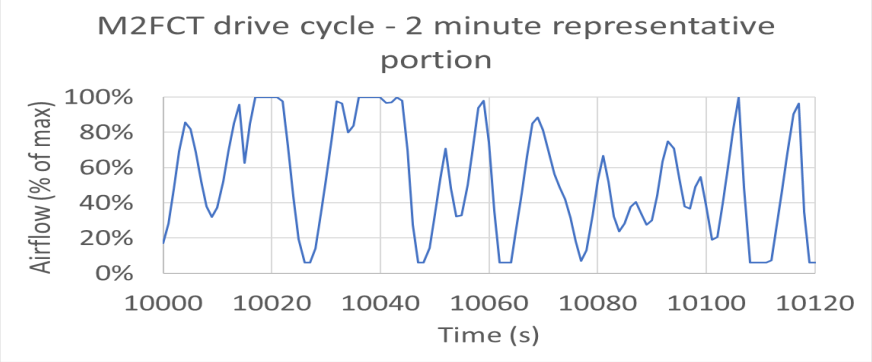

Figure 12:Subset of M2FCT duty cycle

Subtask 1.2: Assess risk benefit, perf targets for water dosing system:

Potential Benefits

A water dosing system offers potential benefits including improved durability, lower operating costs, and reduced parasitic power consumption. Unlike membrane humidifiers, it avoids membrane degradation and air leakage, maintaining consistent water transfer performance. While minor maintenance may be needed for components

like filters and pumps, overall lifecycle costs could be lower than membrane humidifiers, which require full replacement when degraded.

Water dosing also enables evaporative cooling, potentially eliminating the need for an intercooler (if compressor outlet temperatures meet stack requirements) improving efficiency, cost, and packaging. Additionally, the ability to stop water flow and control humidity could eliminate the need for a humidifier bypass valve.

Potential Drawbacks

Potential drawbacks of a water dosing system include challenges in freezing conditions, water availability, and added components. Liquid water can freeze in nozzles, pumps, filters, and plumbing, extending dry-out time before shutdown and requiring extra energy to thaw before startup. Undrained reservoirs may create ice hazards outside the vehicle. Frozen plumbing in water dosing system can block water flow, risking stack degradation due to insufficient humidification. Ensuring adequate water supply across all operating conditions is of concern, likely requiring water recovery and storage.

Water Balance Assessment

The NREL Static Model was used to estimate water dosing requirements for the optimized architecture to meet Ballard's stack inlet humidity targets at 70°C coolant temperature across three DOE operating points. Ambient conditions evaluated included:

- FOA: 40°C, 20% RH, 1.0135 bara
- Cold: -30°C, 5% RH, 1.0135 bara
- High Altitude: 20°C, 50% RH, ~0.84 bara

Water dosing was modeled as direct injection at the compressor inlet. Required dosing rates were calculated using Ballard's humidity targets, and compared to water available at the stack outlet (air + fuel outlet water × separator efficiency).

Results showed water demand exceeded availability at idle and 100% load, while 50% load had surplus water. Cold and high-altitude conditions increased water demand due to lower ambient humidity. At idle, no outlet water is available, requiring a reservoir or increased idle power. Adding a condenser is an option but adds pressure drop.

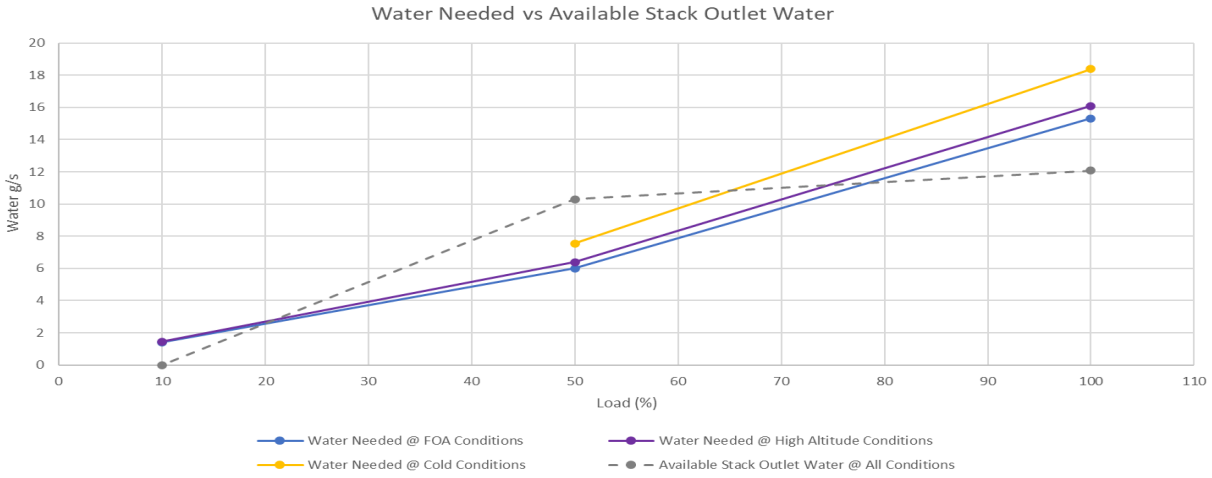

Figure 13: Liquid Water Availability at 70C stack coolant temperature

To close the water gap, the stack coolant temperature was reduced to 60°C, which:

1. Lowered oxidant air temperature, reducing humidification needs.
2. Increased liquid-phase water at the outlet.

With this change, water availability met dosing needs at 50% and 100% loads using only air outlet water. Idle still required a reservoir or higher operating point. The lower coolant temperature adds ~0.7kW of coolant pump power losses at 100% operating point.

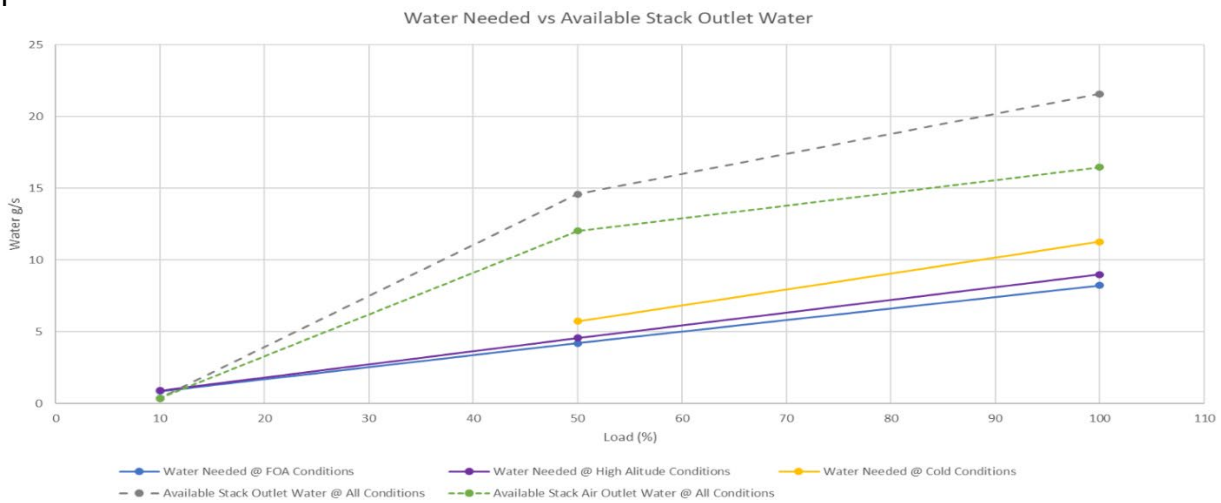

Figure 14: Liquid water availability at 60C stack coolant temperature

Maintaining optimal humidity improves membrane hydration, reducing resistive losses and enhancing performance and durability. Current MEA designs are humidity-sensitive, favoring wet operation. Ballard's provided humidity targets were met in most cases using outlet water and reduced coolant temperature. Idle operation remains a challenge.

Higher temperature operation is a key industry goal. Future MEA designs will aim for better dry tolerance, enabling lower humidity targets, smaller humidifiers or reservoirs, and improved power density and cost.

Subtask 1.3: Proof-of-concept prototype:

Subtask 1.3.1: Build system – Design, Procure, & Fabricate:

Compressor and expander

New compressor and expander designs were developed for this program, as detailed in Task 2 "Improve Roots machine to meet life requirements." To reduce costs, the designs leveraged tooling synergies, particularly in timing gear center distance, resulting in slight deviations from optimized displacements (compressor: 1175cc vs 1188cc; expander: 525cc vs 550cc). Components were sourced externally and assembled manually at Eaton's Marshall, MI campus. Rotor timing was also completed manually due to the absence of dedicated rotor timing assembly tools.

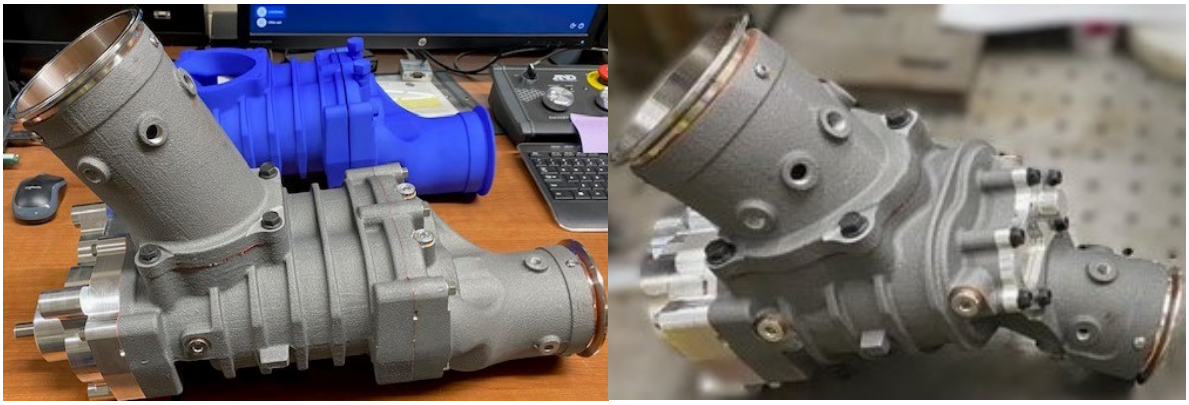

Figure 15: Picture of assembled compressor and expander

Recuperator

The optimized recuperator design specified in task 5 “Maximize recuperator effectiveness with AM technology” was too expensive to procure due to excessive costs in prototype fabrication. To quantify recuperator benefit, an off-the-shelf design with slightly worse performance was purchased from Senior Flexonics. Senior Flexonics’ design is a 34-liter heat exchanger with an array of stainless-steel corrugated tubes.

Figure 16: Assembled Recuperator

Subtask 1.3.2: Create test capability:

Proof-of-concept testing and key metric data collection were conducted at Eaton’s Southfield, MI facility using a mix of custom and commercial components. Due to the high cost of hydrogen infrastructure and fuel cell emulators, no stack or fuel cell emulator was used. Instead, full system analysis, including the fuel cell stack, was performed using a calibrated Dynamic Model. Calibration required individual performance data for each air system component, necessitating four distinct test setups. A modular test bench was developed to accommodate these configurations, as

illustrated in Figure 17.

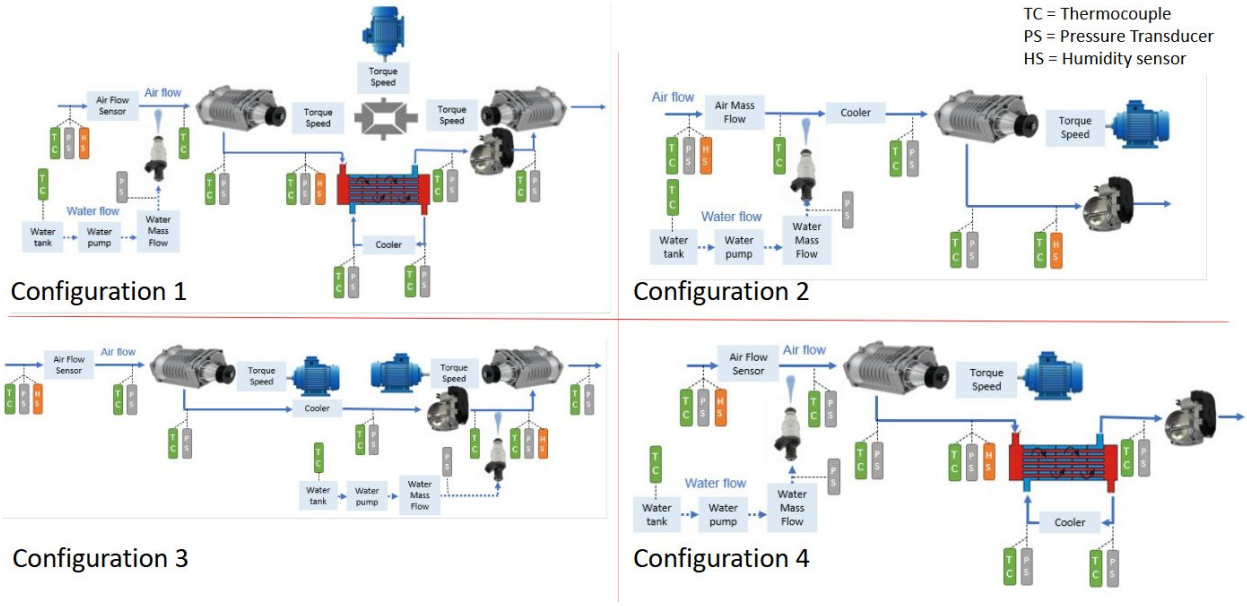

Figure 17: Test configurations
Configuration 1: System and Response Time
Configuration 2: Compressor
Configuration 3: Expander
Configuration 4: Recuperator

Subtask 1.3.2.1: Define methods and procedures:

The initial proof-of-concept test plan included heating and humidification to simulate fuel cell stack conditions without requiring a fuel cell stack. Heating and humidifying air to mimic a stack required more energy than expected. Heater size calculations were confirmed by an environmental test simulation system supplier. Their proposal for the necessary equipment and infrastructure exceeded project budget.

As a result, Key Metrics testing was revised to use four configurations with flow temperatures and humidities that differ from actual conditions. The NREL Dynamic Model was used to adjust results to expected operating conditions and generate reportable values for Electrical Power Consumption, Step Response, and Turndown Ratio. See Table 6 for measured values and analytical corrections.

Table 55: Summary Reporting Approach for Tested Key Metrics

Key Metric	Test Configuration				Measured Parameters	Corrections to Component and System Models	Key Metric Reporting
	1	2	3	4			
Compressor & Expander Efficiency		X	X		Compressor & Expander: • Shaft torque, shaft speed, inlet and outlet temperature, inlet and outlet pressures, humidity.	None.	Report compressor and expander isentropic efficiencies calculated from

					• Isentropic and volumetric efficiencies calculated from measured data.		measured data.
Electrical Power Consumption		X			Compressor: • Shaft torque, shaft speed, inlet and outlet temperatures, inlet and outlet pressures, humidity. • Isentropic and volumetric efficiencies calculated from measured data.	<u>Validate compressor model</u>: Adjust Eaton's proprietary tool predictions for shaft power, outlet temperature, volumetric efficiency, and isentropic efficiency to align with measured data. <u>Create updated compressor maps</u>: Use proprietary tool to simulate compressor performance; create maps including FOA operating points that could not be duplicated in lab. <u>Correct NREL Dynamic Model:</u> Update with validated compressor performance maps.	Report air system net electrical power consumption predicted by NREL Dynamic Model for 3 FOA operating points.
			X		Expander: • Shaft torque, shaft speed, inlet and outlet temperatures, inlet and outlet pressures, humidity. • Isentropic and volumetric efficiencies calculated from measured data.	<u>Validate expander model</u>: Adjust Eaton's proprietary tool predictions for shaft power, outlet temperature, volumetric efficiency, and isentropic efficiency to align with measured data. <u>Create updated expander maps</u>: Use proprietary tool to simulate expander performance; create maps including FOA operating points that could not be duplicated in lab. <u>Correct NREL Dynamic Model:</u> Update with validated expander performance maps.	
				X	Recuperator: • Inlet and outlet temperatures, inlet and outlet pressures, mass flow rate • Heat transfer, effectiveness, and pressure drop calculated from measured data.	<u>Validate recuperator model:</u> Adjust recuperator component model heat transfer, effectiveness, and pressure drop predictions to align with measured data. Use validated model to scale for other recuperator sizes if needed. <u>Correct NREL Dynamic Model:</u> Update with validated recuperator model.	
System Response Time	X				• Mass flow 10-90% response time for 0-100% step command. • Pressures at control valve inlet and outlet. • Fluid conveyance geometries.	<u>Correct NREL Dynamic Model:</u> Temporarily adjust NREL Dynamic Model fluid conveyance geometries to those used in Test Configuration 1. Adjust control valve model to deliver pressure drop aligned with measured data. Adjust step response prediction to align with measured data. Return fluid conveyance geometries to those derived from Proposed System CAD layout.	Report 10-90% mass flow step response time predicted by NREL Dynamic Model.
Turndown Ratio	X				• Mass flow rate at max compressor speed. • Minimum measurable mass flow rate. • Turndown Ratio calculated from measured data.	None.	Report Turndown Ratio calculated from measured data.

Subtask 1.3.2.2 & 1.3.2.3: Design, Procure/fabricate equipment:

The modular test bench was initiated in BP1 and finalized in BP2 using outputs from the static model optimization. Test bench features stainless-steel tubing with sanitary fittings and flexible mounting for the TVS compressor/expander, intercooler, and pressure valves.

Low voltage electrical hardware (data acquisition and control) was assembled on a mobile cart. Wiring was completed using shielded cables and galvanically isolated fixtures to mitigate electrical noise, a known issue at the facility.

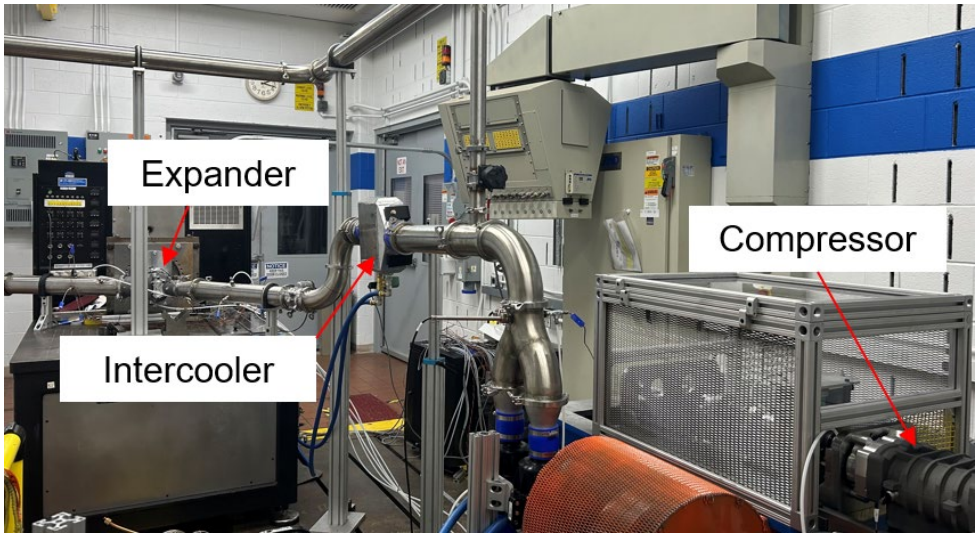

Figure 18: Test cell in expander performance test configuration (Configuration 3)

Subtask 1.3.3 & 1.3.4: Test & Results documentation:

Compressor performance

Compressor performance was mapped across various shaft speeds, pressure ratios, and water dosing rates. Key metrics included isentropic efficiency, volumetric efficiency, specific shaft work, and shaft power. Isentropic efficiency couldn't be calculated with water dosing due to evaporative cooling making it no longer an isentropic process. Specific shaft work was used instead.

All metrics were compared to Eaton's predicted data. Predictions within ±10% of measured values were accepted; others were corrected using test data. The validated data was then used in the Dynamic Model for final Key Metrics analysis.

Dry isentropic efficiency was the first metric evaluated. Due to timing constraints, only a partial map was completed, but all isentropic efficiency measurements met the ±10% accuracy threshold, allowing Eaton's predicted data to be used in the Dynamic Model. See Figure 19 for the corrected performance map.

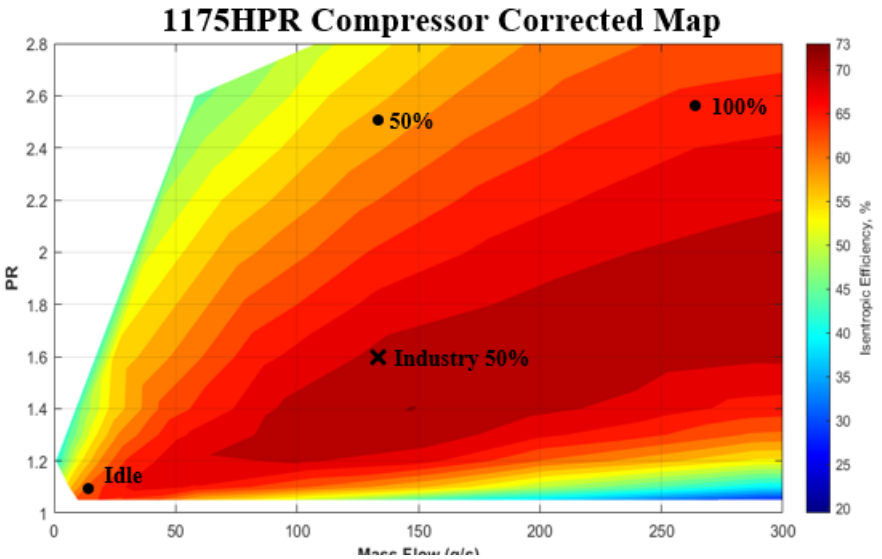

Figure 19: Corrected compressor performance map

Compressor shaft power was the second metric evaluated. Measured values were within ±10% of Eaton's predictions, allowing the use of predicted data in the Dynamic Model. See Figure 20 for shaft power vs. speed.

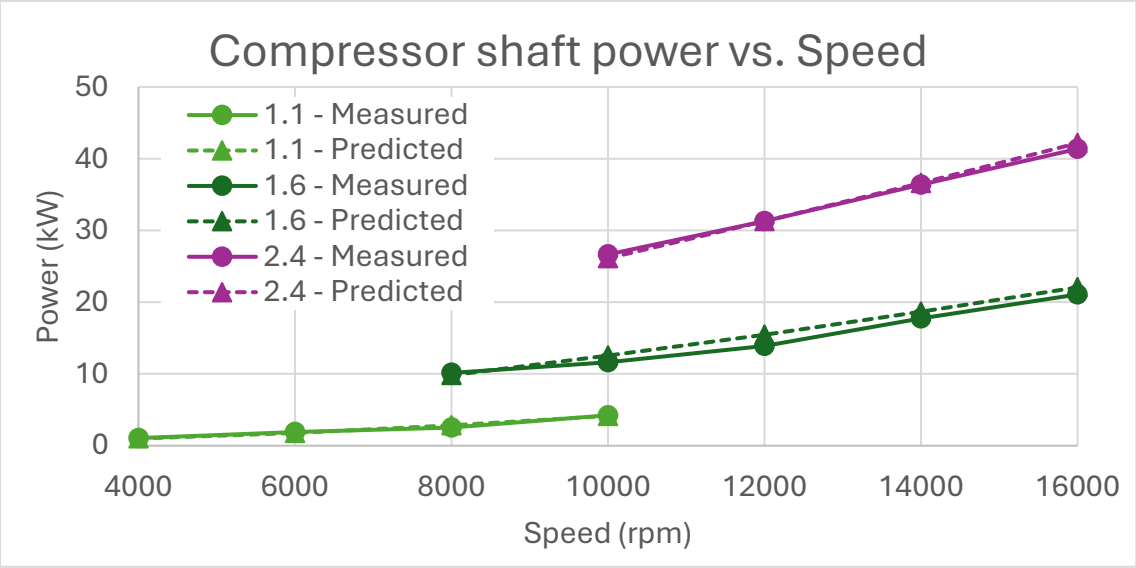

Figure 20: Compressor shaft power test measurements

Compressor volumetric efficiency was the third metric evaluated. Measured values were over 10% lower than Eaton's predictions, especially at low shaft speeds, indicating internal air leakage and reduced mass flow. Error comparisons for volumetric efficiency and mass flow rate are shown in Figures 22 and 23. Map data was corrected to produce performance map in figure 19.

Figure 21: Compressor volumetric efficiency test measurements

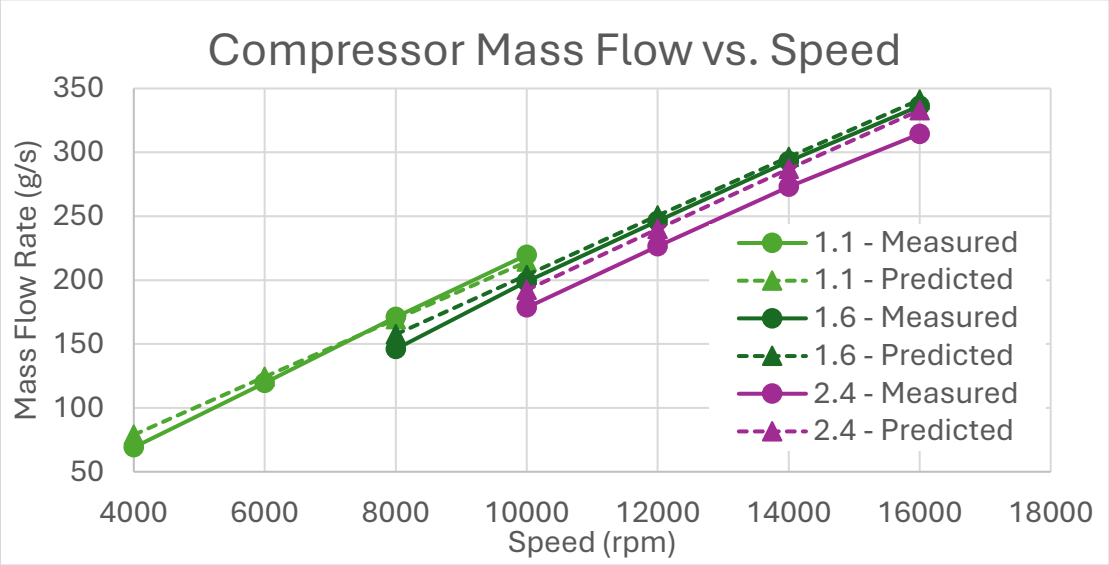

Figure 22: Compressor mass flow test measurements

The impact of liquid water dosing on compressor performance was evaluated, with the most notable effect being a significant drop in outlet air temperature (up to 64°C at 2.0 PR). Temperature readings were carefully managed to avoid errors caused by water coating thermocouples. Measurements were taken at both the compressor outlet and throttle valve inlet, with liquid water separators installed between them to remove residual water. In cases where liquid water was present at the compressor outlet, throttle valve inlet temperatures were higher than compressor outlet, confirming that liquid water caused artificially low readings at the compressor outlet. Temperature comparison graphs are shown below.

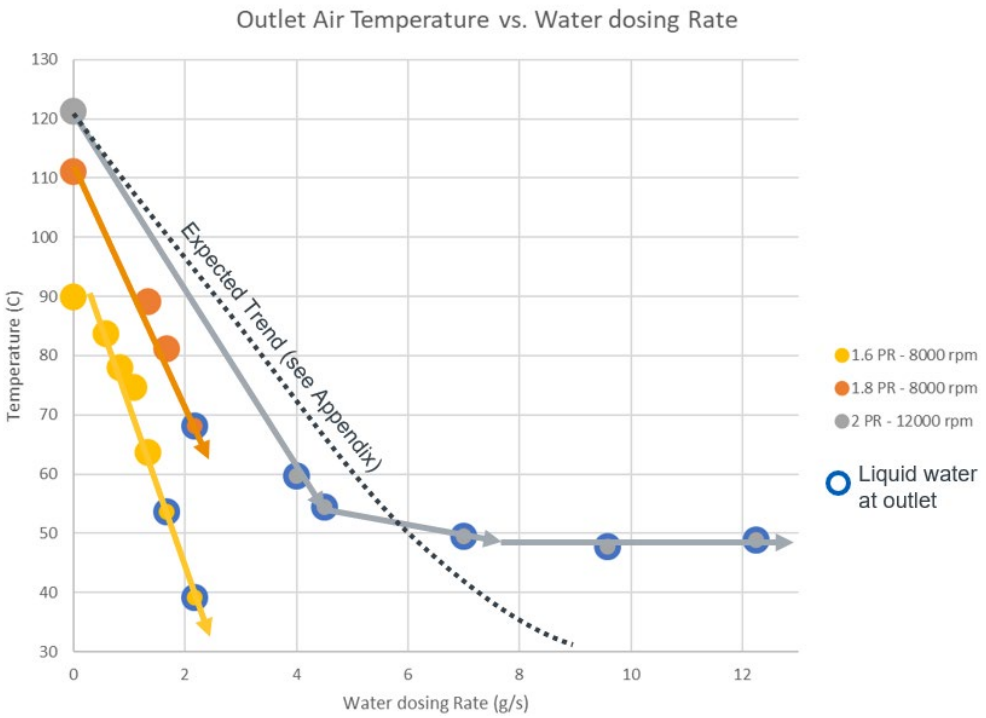

Figure 23: Measured compressor outlet temperature trend with water dosing

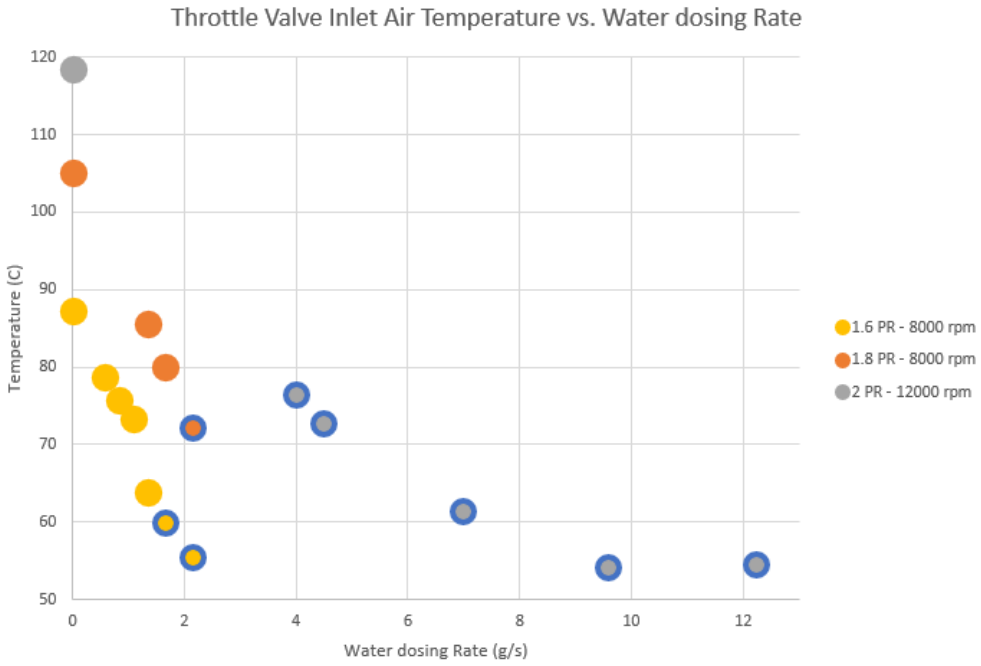

Figure 24: Measured throttle valve inlet air temperature with water dosing

Liquid water dosing also increased compressor volumetric efficiency, indicating reduced internal air leakage. Wet testing of the R1175 compressor showed a ~5% volumetric

efficiency gain, translating to a 10–15 g/s increase in dry air mass flow. These improvements were lower than those seen in earlier tests with R1320 and V400 units. Eaton team suspects a missing design feature, potentially water dosing location inside inlet, present in earlier units but absent in the R1175, may be responsible. Further investigation is needed to identify it. See Figures 25 and 26 for performance graphs.

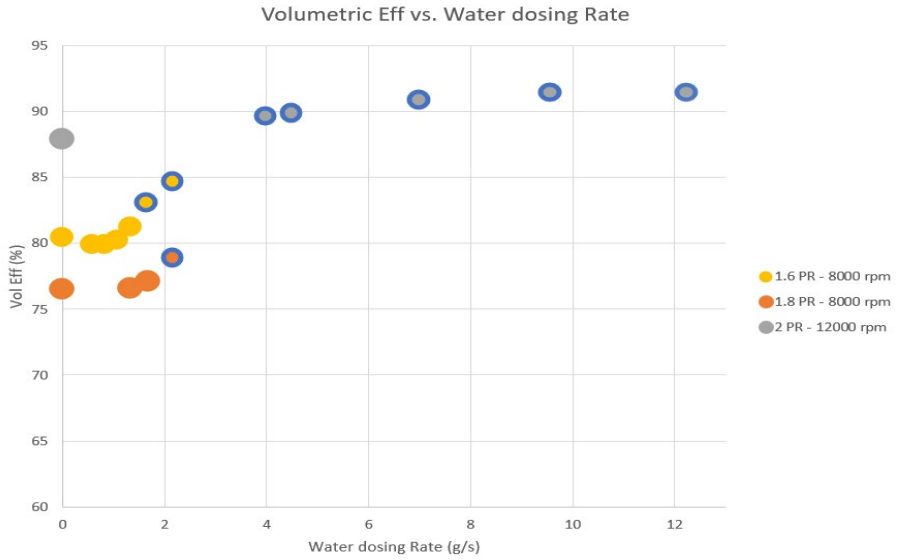

Figure 25: Volumetric Efficiency improvement with water dosing

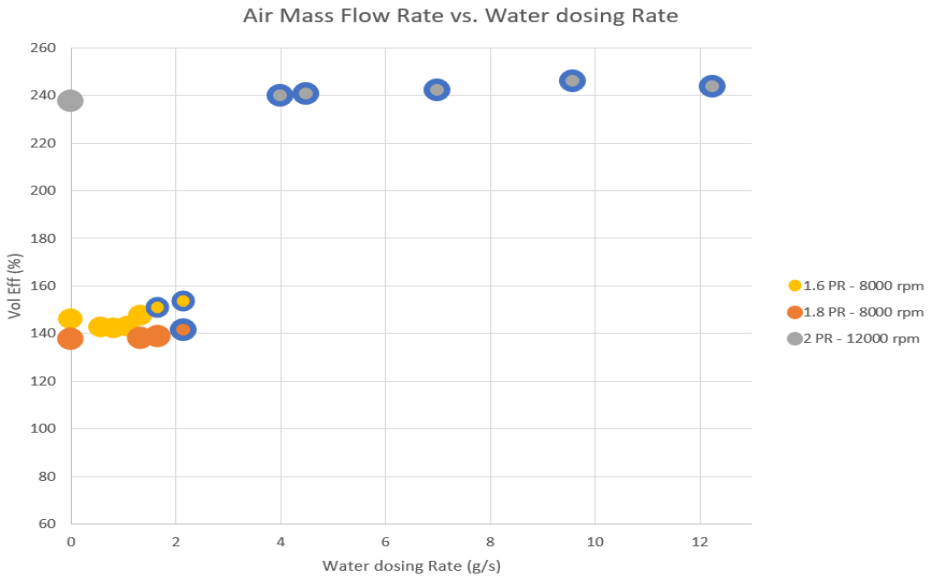

Figure 26: Mass flow rate improvement with liquid water dosing

The final metric analyzed was the effect of water dosing on specific shaft work, used in place of isentropic efficiency during wet testing. The R1175 showed smaller gains than previous tests with R1320 and V400 units, largely due to lower airflow improvements. Specific shaft work vs. dosing rate is shown in Figure 27.

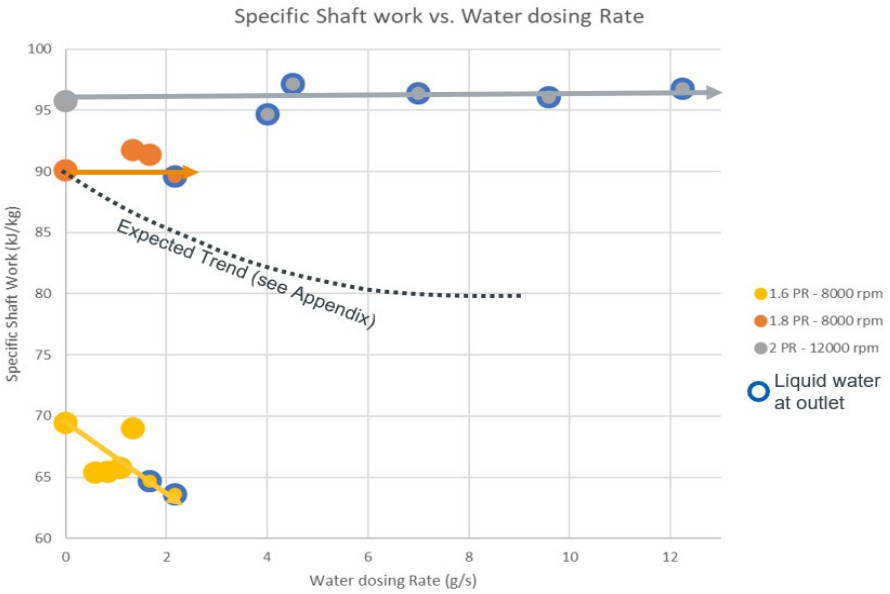

Figure 27: Measured compressor specific shaft work trend with water dosing

Expander performance

Expander performance was tested across various pressure ratios, shaft speeds, and inlet temperatures. Key metrics, isentropic efficiency, shaft power, and volumetric efficiency, were compared to Eaton's predictions. Data within ±10% error was accepted; outliers were corrected and used in the Dynamic Model.

Volumetric efficiency was the first metric analyzed. Test results showed more leakage than expected, requiring higher airflow to maintain pressure ratio. This reduces energy recovery (~1-2kW) and demands greater throttle valve closure in single-shaft systems. Corrected expander volumetric efficiency data was used in the Dynamic Model. See the volumetric efficiency graph below.

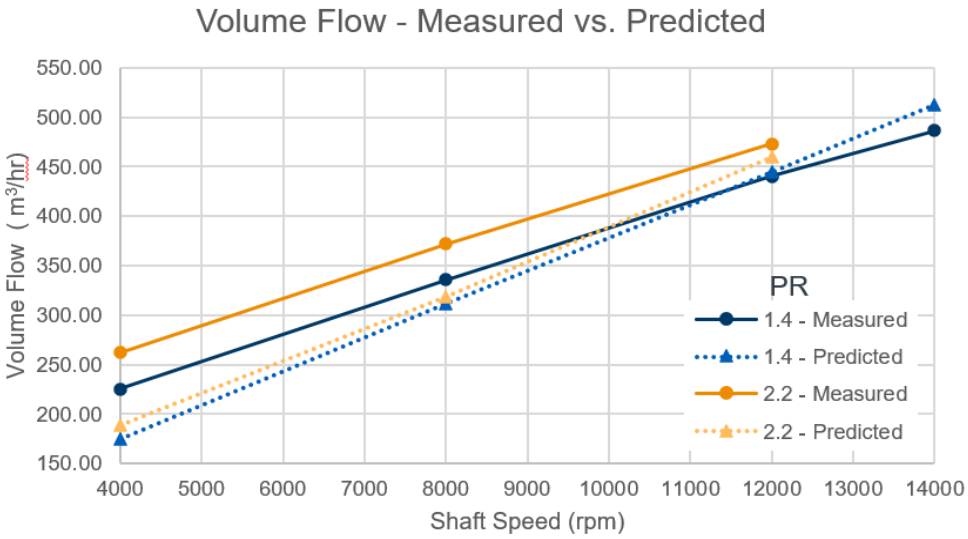

Figure 28: Expander volumetric flow: measured vs. predicted

The second expander metric analyzed was isentropic efficiency. Measured values were over 10% lower than Eaton's predictions, so test data was used to update the performance maps in the Dynamic Model. Efficiency slightly decreased with lower inlet air temperatures, and peak efficiency occurred at higher pressure ratios and mass flow rates than expected (likely due to increased internal leakage). See Figure 29 for the updated performance map.

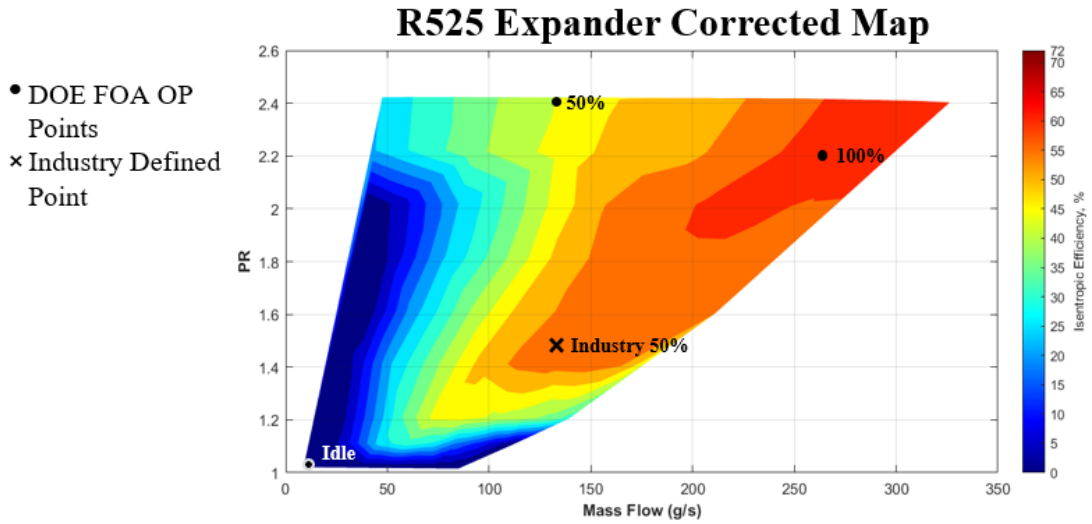

Figure 29: Corrected expander performance map

The final expander metric analyzed was shaft power. Measured values were over 10% lower than Eaton's predictions, so test data was used to update the performance maps in the Dynamic Model. The reduced power recovery may be due to increased internal leakage pushing efficiency islands away from operating points and added shaft seals (added friction drag) not accounted for in Eaton's prediction tool.

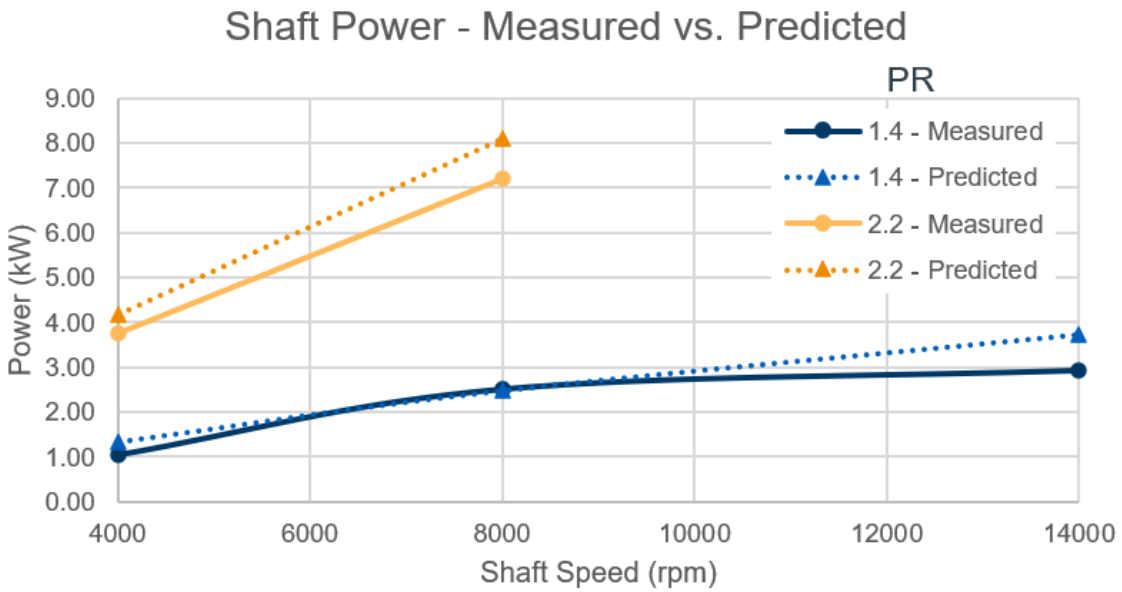

Figure 30: Expander shaft power: measured vs. predicted

During testing the Eaton team noted several findings that are perceived to be important, although not directly tied to the key metrics listed in the FOA. The first finding was rust inside the compressor due to water dosing. Rust was observed on the rotor, traced back to steel rotor shaft seal that corroded and contaminated the rotor bore. This was a design oversight from reusing production seals to reduce costs. Future designs will use non-corrosive materials for seal housings.

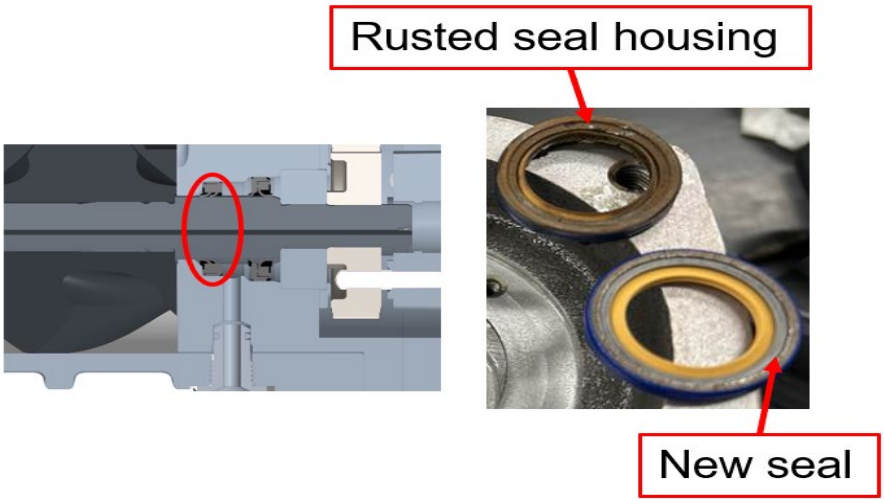

Figure 31: Compressor post-test teardown: rusted shaft seal housing

Another key finding was that the shaft seal isolating the rotor bore from the seal vent had shifted along the shaft, as indicated by wear marks. This issue creates a leak and could be the cause for the reduction in flow. Eaton suspects this was caused by a pressure

spike during testing. Future designs will include mechanical retention, such as a snap ring or spacer, to prevent seal movement. See Figure 32 for examples.

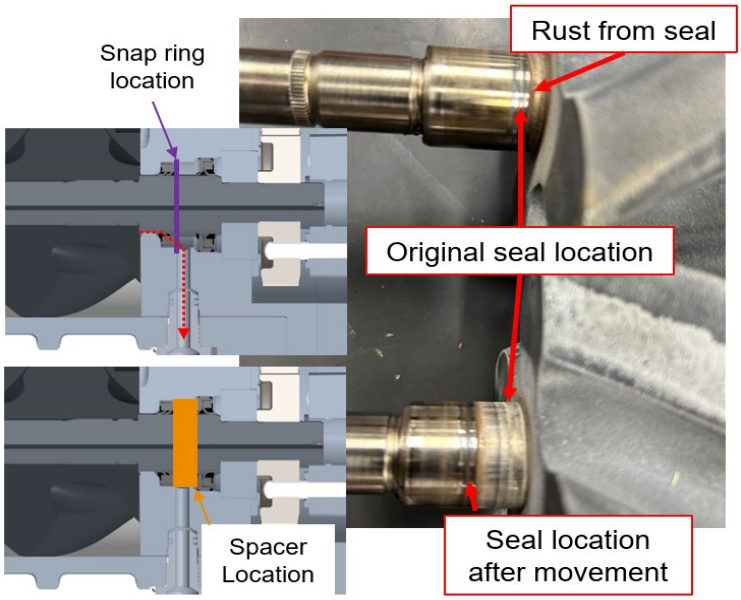

Figure 32: Compressor post-test teardown: shaft seal movement

A third key finding was significant wear on the compressor rotor lobe abradable coating, likely caused by timing errors during manual assembly. Due to the housing design, proper tooling for rotor timing wasn't available, increasing the risk of misalignment. This wear may have reduced volumetric efficiency. Any future production compressors will include dedicated tooling to enable use of Eaton's rotor timing machine.

Figure 33: Compressor post-test teardown: rotor wear

Recent compressor testing showed reduced water dosing effectiveness. Tap water used in testing left calcium deposits where water evaporated on the rotor bore, visually indicating evaporation zones. Unlike previous tests (R1320 and V400), evaporation was concentrated near the outlet rather than along the rotor length. Greater surface area for evaporation improves performance and helps seal internal leakage. Changes in surface area coverage could be due to differences in water doser location. Although hard to see, a white calcium layer is visible in Figure 34; parts are available for inspection as well.

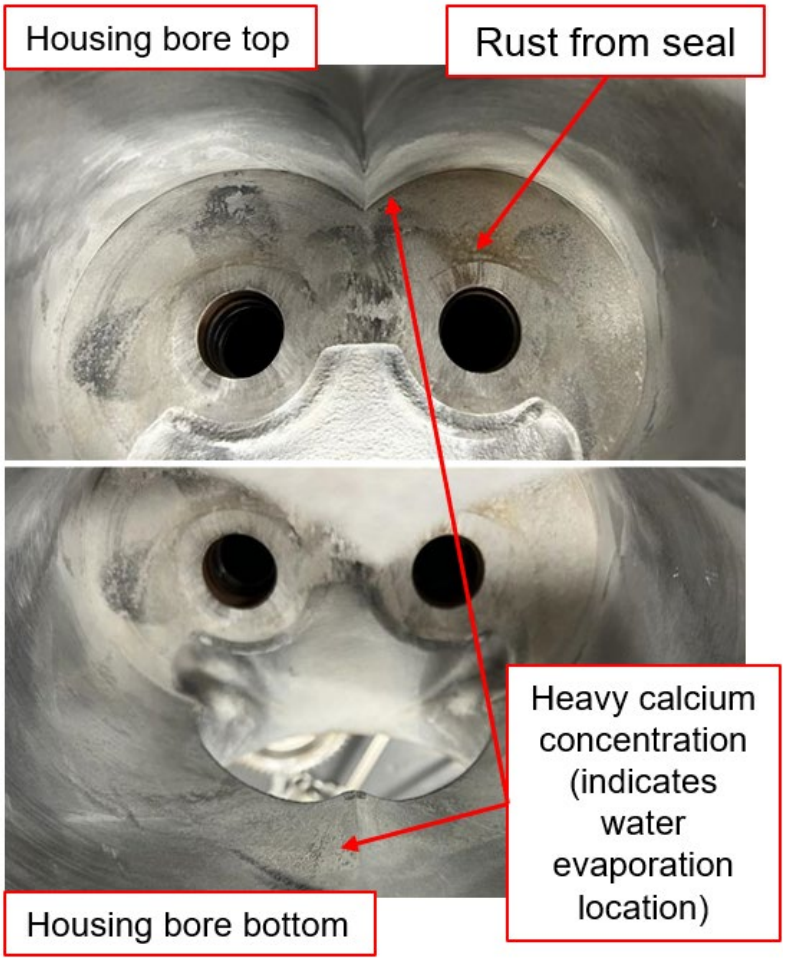

Figure 34: Compressor post-test teardown: water evaporation location

The Eaton team also studied how expander inlet air temperature affects energy recovery. Tests were run at constant shaft speed and pressure ratio while varying inlet temperature. Results showed no increase in recovered power with higher inlet temperatures, indicating the expander does not directly recover thermal energy.

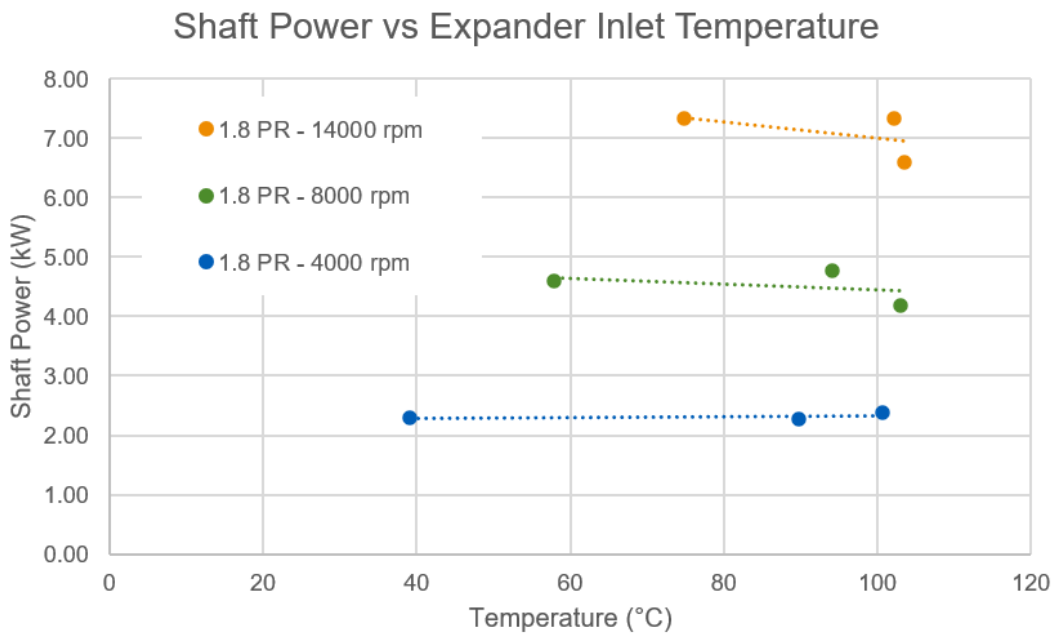

Figure 35: Measured expander power vs inlet air temperature

However, higher expander inlet air temperatures increase volumetric flow rate (for a constant mass flow), which can enhance energy recovery. As flow increases, expander inlet air pressure rises, prompting the throttle valve to open to maintain stack pressure. This results in a higher-pressure ratio across the expander, allowing it to recover more power.

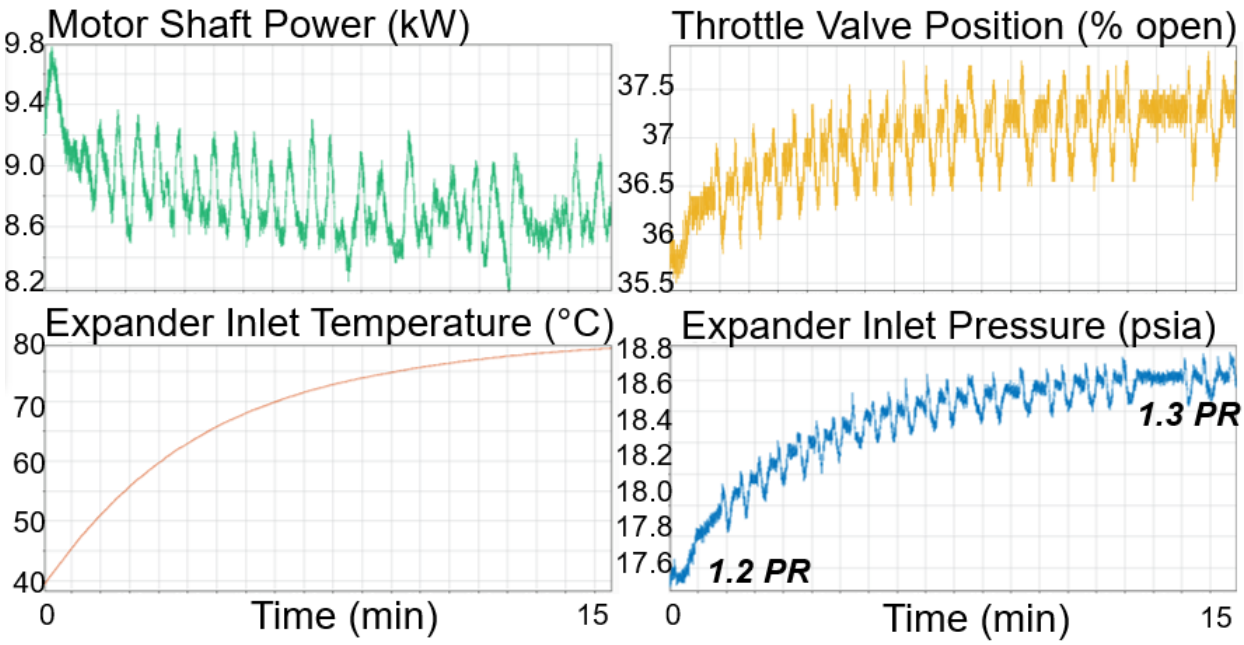

Figure 36: Expander inlet air temperature system effects

During step changes or sudden throttle valve closures, vacuum pressures were observed at the expander inlet. This likely occurred because the expander, rigidly connected to the compressor, spun at higher speeds than required for the given inlet airflow, creating vacuum. In this condition, the motor supplied power to the expander. To prevent this, a one-way clutch (e.g., ramp roller) could be added between the motor and expander shafts, allowing power flow only from the expander to the motor and avoiding vacuum formation.

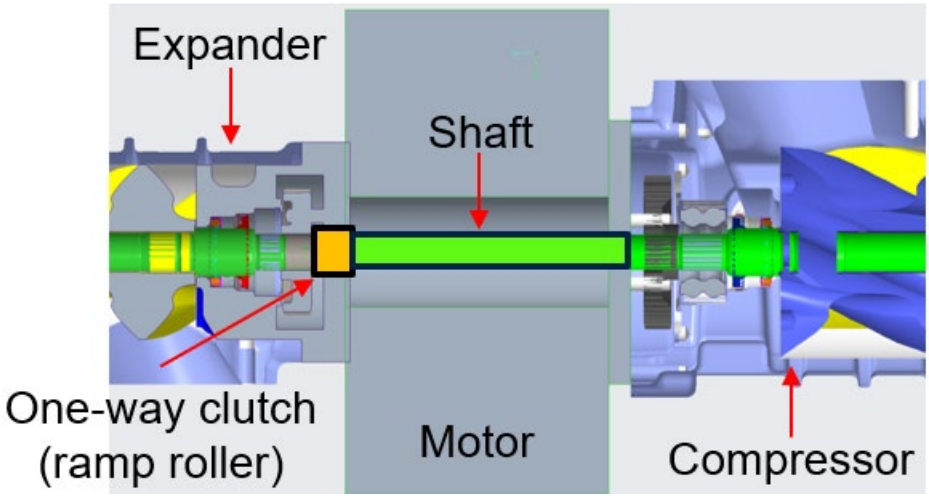

Figure 37: One-way clutch implementation example

Final results

Final key metrics for electrical power consumption were gathered using three step-change profiles used in calibration and a period of idle operation. Step response time matched test results at 0.62 seconds (10–90% mass flow). Net electrical power consumption was 37 kW (100%), 8 kW (50%), and 0.22 kW (idle), all higher than static model predictions (24.08 kW, 6.8 kW, and 0.21 kW). This was contrary to expectations with the updated compressor and expander designs, though 50% and idle values remained below project targets.

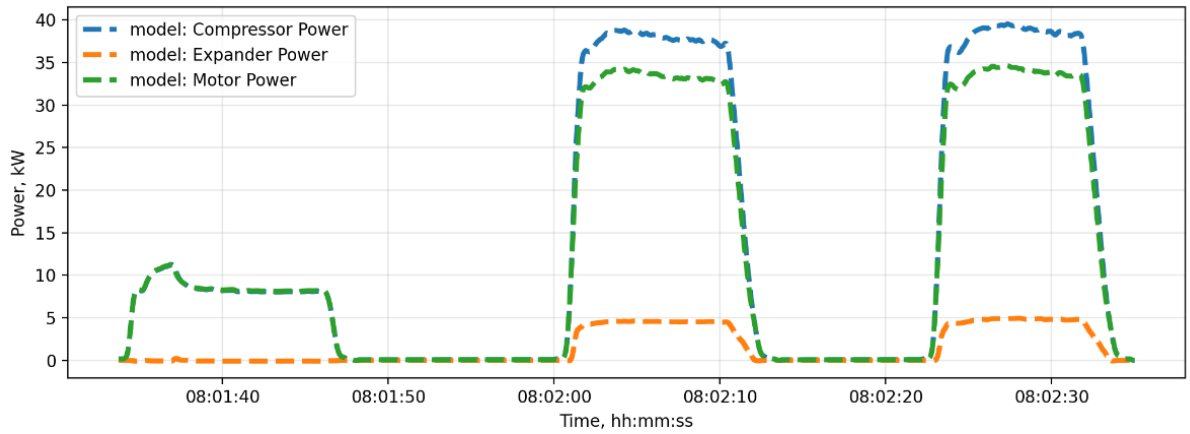

Figure 38: Final component power consumption results

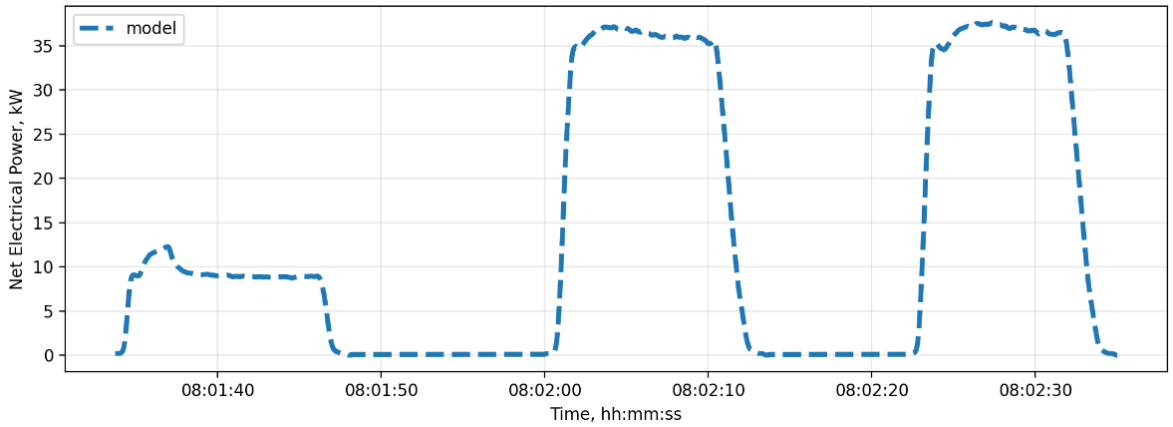

Figure 39: Final net electrical power consumption results

A major factor in the increased electrical power consumption was the significant drop in recovered energy from the expander. This reduction is likely due to increased air leakage in both the compressor and expander, and higher friction losses from additional double lip seals in the expander assembly.

Leakage in both components lowers expander inlet pressure, reducing shaft power. Expander leakage requires more airflow to maintain pressure, while compressor leakage forces it to spin faster to meet flow requirements. Since both are on a shared shaft, the expander also spins faster, demanding more airflow to sustain pressure, thus lowering expander inlet air pressure.

Eaton's performance prediction tool only accounted for a single set of seals. The final design included an additional set with a vent (for oil free air), which increased friction losses not reflected in simulations.

Additionally, expected power gains from liquid water dosing were not realized with the updated R1175 compressor. This may be due to differences in water injection orientation. Previous tests injected water horizontally across the rotor cavity inlet, while R1175 testing used vertical injection. The horizontal method may have provided better water distribution and surface coverage, enhancing sealing and evaporation.

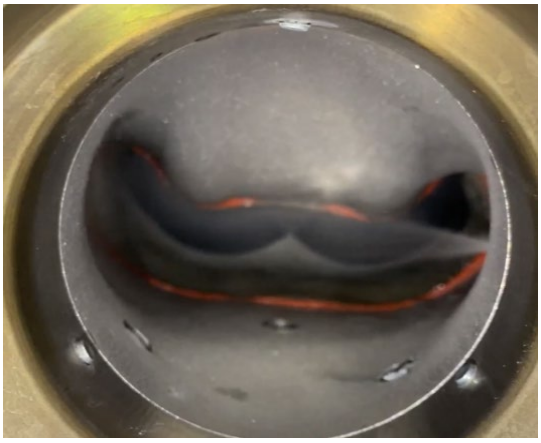

Figure 40: Horizontal spray pattern

Additionally, the compressor outlet orientation may have affected the effectiveness of liquid water dosing. R1175 testing used a downward-facing outlet, while previous V400 tests had an upward-facing outlet, possibly allowing water to pool in the rotor bore and improve sealing. However, similar results were not observed with the R1320, which also had a downward-facing outlet, casting doubt on this hypothesis.

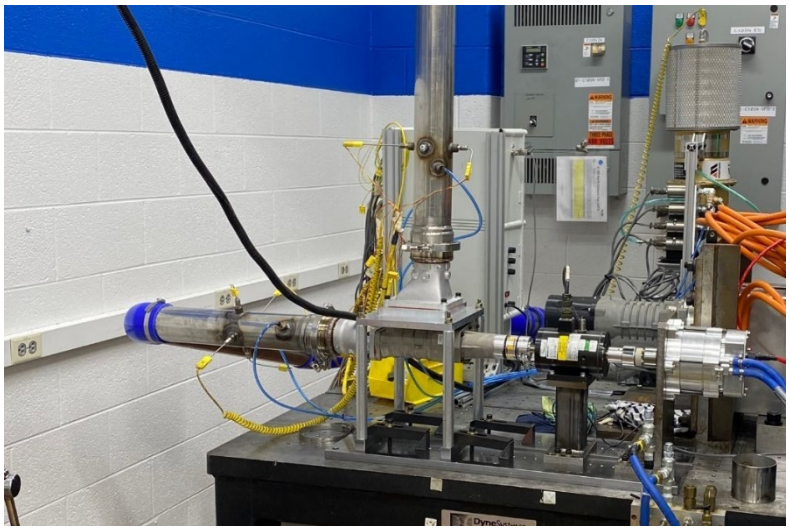

Figure 41: V400 testing layout at Eaton Southfield

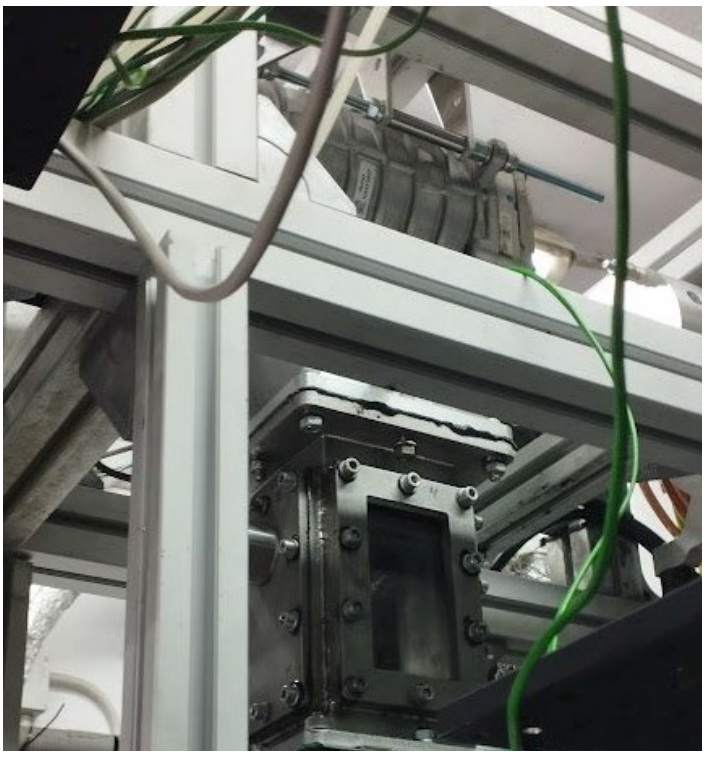

Figure 42: R1320 testing layout at CMT

Task 2 Improve roots machines to meet life requirement:

The NextGen TVS machines, designed for fuel cell air systems, differ significantly from Eaton's internal combustion engine boosting products, particularly in pressure ratio capabilities and the positioning of efficiency islands on their operating maps.

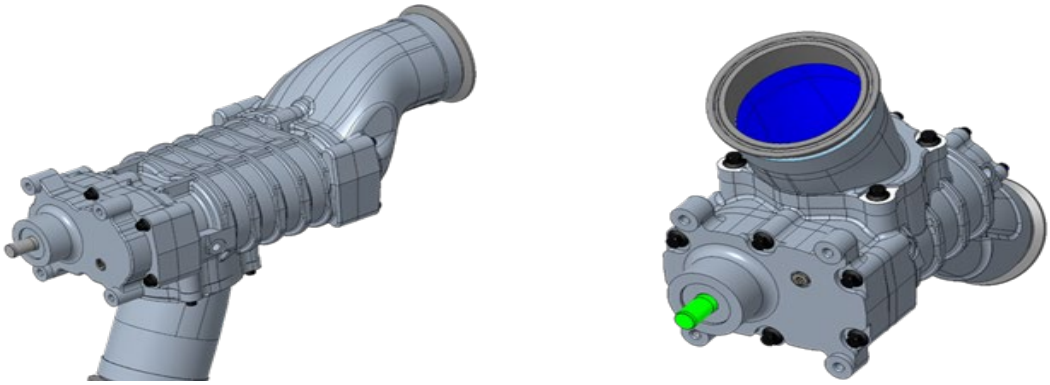

Figure 43: Prototype NextGen TVS machines - R1175 compressor (left) and R525 expander (right)

The NextGen compressor was designed with optimized housing and rotor geometries to increase internal compression and reduce outlet turbulence. Rotor profiles were revised to shift the peak efficiency island to desired operating points. The expander design was guided by prior Eaton DOE work, testing from this program, and Eaton's proprietary TVS tool, with emphasis on inlet port geometry for high enthalpy flow and rotor shapes tailored for expansion.

Figure 44 shows the simulated NextGen compressor map overlaid with Ballard's expected operating line. Estimated peak efficiencies are 73% for the R1175 compressor and 70% for the R525 expander.

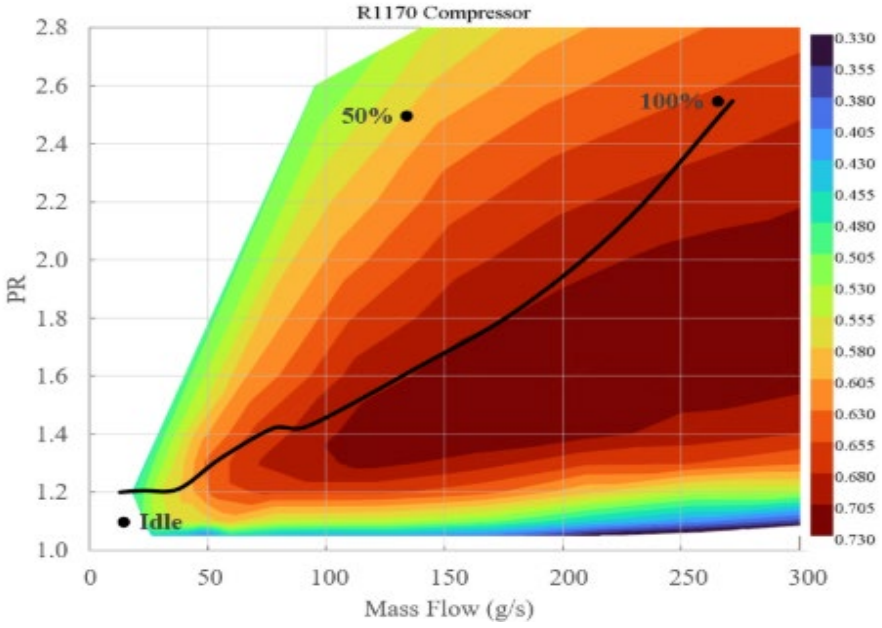

Figure 44: Preliminary NextGen R1175 compressor map with Ballard operating line and FOA operating points

Durability and reliability were also key design considerations for the NextGen TVS machines. Critical wear components (bearings, shafts, seals, and gears) were evaluated using compressor and expander duty cycles derived from M2FCT data (Subtask 1.1.6). Initial bearing life estimates met FOA durability targets, but required larger bearings than those used in passenger car applications. These larger components impacted inlet and outlet flow paths, potentially affecting efficiency. Prototype hardware incorporated these geometric changes to reflect expected performance.

The duty cycles lacked dynamic loading data due to limitations in Subtask 1.1.6. Plans to use the Dynamic model for a higher fidelity durability assessment were in plan, but unfortunately was not completed due to project timing. The study performed also did not account for loads from imbalance or shaft resonance, which are typically addressed in later design stages. A more detailed bearing study and validation would be completed before any future production.

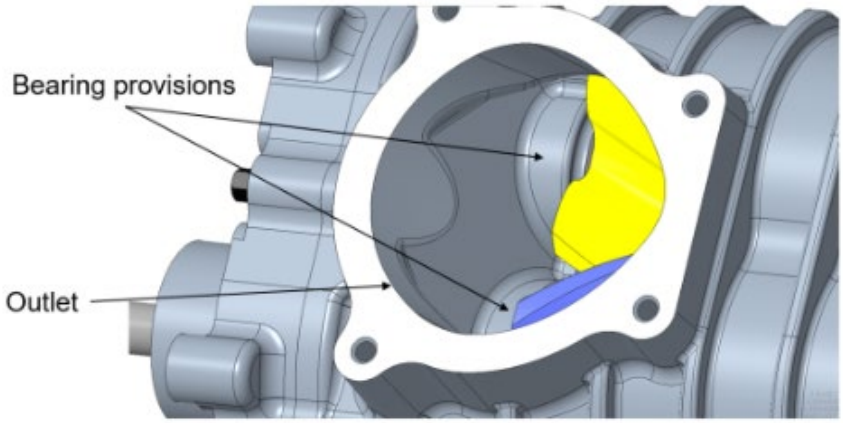

Figure 45: Bearing space claim impingement upon outlet flow path

Standard production supercharger timing gears were used. Gears were evaluated using MASTA software in Task 3 and found suitable in terms of life and noise. Seal life would require joint analysis by Eaton and the supplier during product development. TVS machine performance is not expected to be affected by Startup/Shutdown Cycles metric, due to use of roller bearings. Bearing damage was limited to duty cycle effects, assuming proper lubrication during startup and shutdown.

To prevent oil contamination, Eaton applied a proven double-seal strategy from other TVS applications. One seal isolates the oil cavity, the other the air cavity, with a vented space between the two to drain any leakage (water or oil). This approach has been validated in passenger car systems handling liquid water and high exhaust gas recirculation.

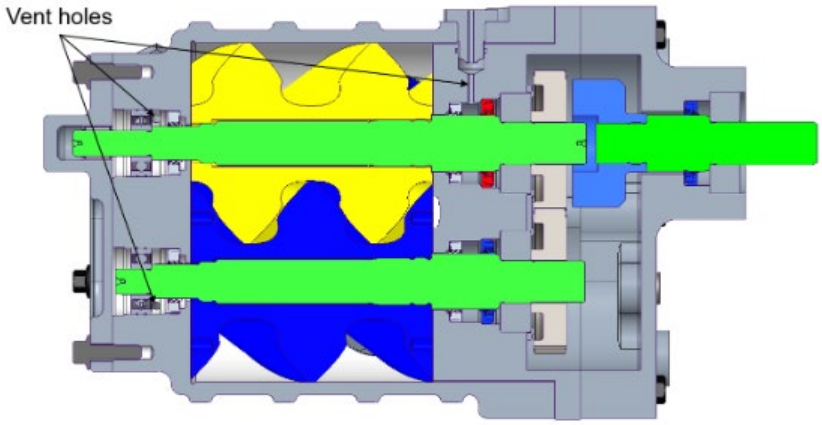

Figure 46: Shaft sealing strategy to prevent oil contamination in airflow

Due to expected water content in the fuel cell air stream, corrosion mitigation was necessary for components like rotor shafts, rotor forms, and internal air cavity surfaces. Electroless nickel plating was considered for rotor shafts to enhance corrosion resistance while preserving seal compatibility. Aluminum rotor forms were protected using anodizing and abradable coatings (compatible with Ballard's material requirements). Housing, inlet, and outlet surfaces, also aluminum, were anodized to protect machined features while maintaining tight design tolerances.

Task 3 Maximize geartrain efficiency:

Subtask 3.1: Design max efficiency tooth forms

Initial system architecture concepts included a differential gearbox to allow mechanical transmission of the recovered power in the expander to the compressor, while also allowing the compressor and expander to spin at optimal shaft speeds. An application specific differential gearbox design was required to calculate an appropriate loss model to use in the static model optimization.
An initial sizing study for the differential gearbox was conducted, including creation of a 3D CAD model and a model in SMT MASTA gearing systems analysis software. Once the initial sizing study showed feasibility, mechanical power transmission loss models were created for use in the NREL Static Model.

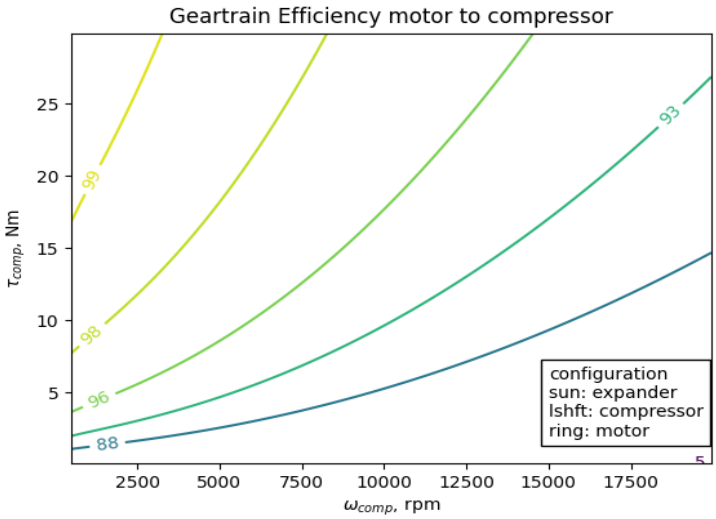

Figure 47: Predicted differential gearbox efficiency

Component life analysis was based on the M2FCT duty cycle with a gearbox differential ratio of 2.32 and a 69 Nm maximum torque from early system operating point predictions.

MASTA analysis of these conditions indicated design changes were needed to meet strength and life requirements. Increasing planetary gear diameter would have compromised gearbox size and packaging, so the planetary set was redesigned from three to five planet gears. This improved reliability and power density without increasing space claim. The updated design met all durability and reliability targets, adding 3.2 kg and increasing cost by 56% over the initial concept. Component life analysis was not re-visited at the end of the program since the differential gearbox was not in the optimum architecture.

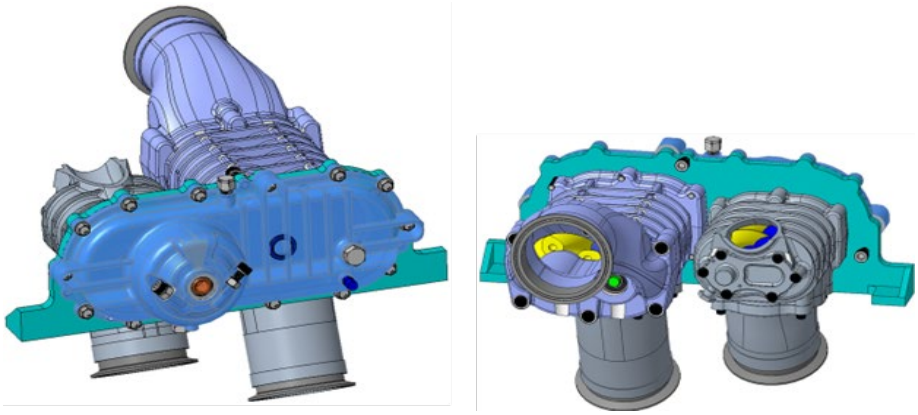

Figure 48: Differential gearbox with compressor and expander attached

Differential gearbox cooling and lubrication strategies were defined with oil channels and passages added to the enclosure and ring gear for proper lubrication of planet gears and bearings. Oil baffles were included to reduce windage losses and improve efficiency. A literature review identified optimal clearances of 1–1.5 mm between

rotating and stationary components, which were applied to the design with allowances for prototype tolerances. Adjustable oil flow orifices were added to the main case for experimental fine-tuning during testing. Additionally, finite element analysis for complex components like the planet carrier and ring gear shaft showed low stress and deformation than expected, suggesting potential for weight reduction.

Gearbox noise was assessed based on gear excitation. Initial microgeometry modifications were applied, and loaded tooth contact analysis was performed using MASTA with a duty cycle-based load spectrum. Transmission error (TE), the primary noise indicator, was analyzed across gear meshes. First harmonic TE values were compared to Eaton's high-speed, low-load design guidelines and showed favorable results. Table 7 presents the noise excitation safety factor, calculated as the ratio of allowable to maximum TE first harmonic across the load spectrum.

Although the NREL Static Model favored single-shaft transmission, the differential gearbox was initially planned for BP2 testing. Due to budget and timing constraints, testing was removed but could be pursued in future funding opportunities.

Table 6: Safety factor of TE first harmonic relative to Eaton design guidelines

	Compressor Timing Gears	Expander Timing Gears	Layshaft Gears	Differential - Sun/Planet mesh	Differential - Planet/Ring Mesh
Safety factor of noise excitation	1.8	1.8	2.8	4.3	14.7

Subtask 3.2: Estimate cost and manufacturability:

Eaton Corporation has a strong U.S. manufacturing footprint, with key facilities in Michigan, Indiana, Georgia, and North Carolina. The Kings Mountain gear plant and South Bend forging facility are central to geartrain production. Superchargers are built in Athens, GA, and designed/tested in Marshall, MI, making it feasible to assemble the geartrain at the same location, leveraging existing expertise and infrastructure.

Eaton can produce core components like gears and shafts in-house, while sourcing others (e.g., bearings, enclosures) through its supply chain. Eaton also has established capabilities for assembly, distribution, and service across the U.S. However, scaling to high volumes (e.g., 100,000 units/year) would require investment in new equipment and a dedicated assembly line.

Task 4 Optimize electric drive system:

Subtask 4.1: Create motor model for system sims using TARDEC results:

To improve accuracy in static model optimization, application-specific motor + inverter efficiency maps were developed. Motor efficiency peaks near the base speed and rated torque, while inverter efficiency is highest at low torque and high speed. Since different air system architectures operate under varying conditions, 13 unique motor + inverter

efficiency maps were created and assigned to each air system architecture to ensure accurate power consumption estimates.

The optimal single-shaft architecture used a 39 kW radial flux motor (34 Nm, 14,000 rpm max speed) paired with a silicon carbide (SiC) inverter. Radial flux was chosen over axial flux due to similar efficiency at significantly lower cost.

Motor Torque (Nm)	Speed (RPM) Motor + Inverter Map														
	1400	3800	5000	6200	7100	7400	7700	8900	10100	11300	11900	12500	13100	13700	14000
34	0.844	0.907	0.917	0.924	0.927	0.928	0.929	0.930	0.930						
32	0.847	0.909	0.919	0.925	0.929	0.930	0.931	0.932	0.932	0.931					
30	0.853	0.912	0.921	0.928	0.931	0.932	0.933	0.934	0.934	0.933	0.931	0.931			
28	0.855	0.913	0.922	0.928	0.932	0.933	0.934	0.935	0.934	0.933	0.932	0.932	0.930		
26	0.858	0.915	0.924	0.930	0.933	0.934	0.935	0.936	0.936	0.935	0.933	0.933	0.932	0.931	0.930
24	0.863	0.917	0.926	0.932	0.935	0.936	0.937	0.937	0.937	0.936	0.935	0.934	0.933	0.932	0.932
22	0.868	0.919	0.928	0.933	0.936	0.937	0.938	0.938	0.938	0.937	0.936	0.935	0.934	0.933	0.932
20	0.871	0.921	0.929	0.934	0.937	0.937	0.938	0.939	0.938	0.937	0.936	0.935	0.934	0.933	0.932
18	0.873	0.921	0.929	0.934	0.937	0.938	0.938	0.939	0.938	0.937	0.935	0.935	0.933	0.933	0.932
16	0.876	0.922	0.929	0.934	0.937	0.937	0.938	0.938	0.938	0.936	0.935	0.934	0.932	0.932	0.931
14	0.880	0.922	0.929	0.933	0.935	0.936	0.937	0.937	0.936	0.933	0.932	0.931	0.929	0.928	0.927
12	0.880	0.922	0.928	0.932	0.934	0.935	0.936	0.935	0.934	0.932	0.930	0.929	0.927	0.926	0.925
10	0.882	0.921	0.926	0.930	0.931	0.932	0.932	0.931	0.930	0.927	0.925	0.924	0.921	0.920	0.919
8	0.881	0.917	0.922	0.925	0.926	0.926	0.926	0.925	0.922	0.919	0.916	0.915	0.912	0.910	0.908
6	0.878	0.910	0.914	0.915	0.915	0.915	0.915	0.912	0.909	0.904	0.901	0.898	0.895	0.892	0.890
4	0.867	0.894	0.895	0.894	0.893	0.892	0.892	0.886	0.881	0.874	0.869	0.865	0.861	0.857	0.854
2	0.829	0.844	0.841	0.835	0.829	0.827	0.825	0.814	0.804	0.791	0.783	0.777	0.769	0.762	0.758

Figure 49: Motor + inverter efficiency map

Subtask 4.2: Analyze and optimize component lives:

Duty cycle data was derived from the M2FCT fuel cell duty cycle and the NREL Static Model. Motor duty cycles showed load profiles similar to those of passenger car traction motors. By adjusting passenger car reliability data, the reliability for this application is estimated as 90% for the 25,000-hour (1.2M mile) life target.

Key design considerations included time spent at peak torque, power, or speed. Extended operation in these regions (>30 seconds) increases complexity, cost, and manufacturing challenges due to tighter tolerances. Benchmarking was used to estimate cost, performance, and life of the recommended solution, though detailed risk and lifecycle analyses were beyond the scope of this study.

Subtask 4.3: Estimate cost and manufacturability:

Motor and inverter designs were guided by engineering judgment and performance targets. Cost and weight estimates were based on benchmarking studies of electric passenger vehicles, covering components such as stator cores, cooling jackets, windings, rotor assemblies, power modules, control circuitry, housings, DC bus capacitors, and busbars.

A detailed manufacturability analysis was not included. Radial flux motors benefit from established manufacturing practices, while silicon carbide (SiC) inverters, though promising, face ongoing challenges in materials, application development, and processing. Leading semiconductor manufacturers are currently sampling SiC products, with initial automotive production expected in the next product cycle. Some products are already seen in racing applications.

Task 5 Maximize recuperator effectiveness with AM technology:

Subtask 5.1 & 5.2: Optimize heat transfer and flow performance & Size recuperator:

Before the contract began, Eaton used internal R&D funding to explore additive manufacturing (AM) for recuperator designs. The study found that conventional methods (e.g., rolled sheet forming and joining) were ultimately better suited to meet performance targets. Eaton designed a crossflow plate-fin recuperator using proprietary tools and CFD analysis, which met initial flow and temperature goals.

Although the design met preliminary targets, further optimization was desired. Due to resource constraints, Eaton sought proposals from six heat exchanger manufacturers, receiving no-quotes from each manufacturer. Eaton then engaged Purdue University, which proposed a design optimization study and prototype fabrication using conventional technologies.

Purdue evaluated three heat exchanger types (plate-fin with offset strip fins, Chevron-corrugated plate, and flat plate) using a Python-based model. Heat transfer was calculated via the e-NTU method, and pressure drop via type-specific equations. A multi-objective optimization using NSGA-II was conducted, focusing on pressure drop and effectiveness. Results are summarized below.

Plate Type	Flow Configuration	Volume [Liters]	Performance	
			Effectiveness [-]	Total Pressure Drop [Pa]
Offset Strip Fins	Cross-Flow	18	0.74	460
	Counter-Flow	18	0.85	1430
		28	0.89	1010
Chevron-Corrugated*	Counter-Flow	28	0.71	282
			0.74	377
Flat Plate	Counter-Flow	28	0.64	25

Figure 50: Recuperator optimization study results

Subtask 5.3: Estimate cost and manufacturability:

A detailed recuperator manufacturability assessment was not conducted since the recuperator is using existing heat exchanger technology that is widely used in industry today. Cost was estimated by analysis of today's production system of similar size.

Task 6 System cost and manufacturability:

System cost for each element (compressor, expander, motor/inverter, water dosing system) was estimated with data from today's production solutions (or similar solutions)

and added together to form a total system cost estimate. Estimates were based on 100,000 units per year assumption given by DOE. No manufacturability concerns were identified throughout the study as all the components are already in production (inverter technology is in small scale production). Additional details can be found in the "Estimate cost and manufacturability" section of each component subtask in this report.

Table 6: System Cost Estimate

Component	Cost estimate (USD)
Motor	305
Inverter	507
Compressor	952
Expander	550
Water Doser	869
Total	3183

Task 7 Project Management and Planning:

Subtask 7.1: Go/NoGo Decision Point 1 M16:

Go/No go decision point 1 was based on results from the NREL static model optimization study and component design studies. Results from these studies indicated performance meeting or exceeding targets for all but the 50% power consumption target (shown in table 8). 50% power consumption target was de-emphasized after DOE identified that the 50% operating point specified in FOA was unrealistic.

Table 7: Go/No go decision performance outlook

Key Metric		DOE 2030 Target	Status as of August 2023
Motor + Motor Controller Efficiency	**100% Flow**	92%	93.5%
	50% Flow	92%	93.6%
	Idle	80%	82.3%
Compressor/Expander Efficiency	**100% Flow**	75/70 %	66/63% See Electrical Power Consumption below.
	50% Flow	80/80 %	58/47% See Electrical Power Consumption below.
	Idle	62/60 %	53/28% See Electrical Power Consumption below.
System Response Time		2 seconds	0.4 seconds
Durability		25,000 hours	Air system reliability 52% at 25,000 hours
Reliability		50,000 MBRC	Air system MBRC estimate 1.84M
Number of Startup Shutdown Cycles		50,000	See discussion in Task 2.
Noise at Idle		65 dB-A @ 1m	Between 63.6 and 67.2 dB-A.
System Cost		$3600	$3183

System Volume		0.25 L/kW	0.24 L/kW
System Weight		0.5 kg/kW	0.16 kg/kW
Turndown Ratio		20	32.8 or greater
System Efficiency Expressed as Air System Electrical Power Consumption for 300kW Fuel Cell:			
Electrical Power Consumption	**100% Flow**	27.9 kW	24.5 kW
	50% Flow	10.8 kW	14.7 kW
	Idle	0.32 kW	0.21 kW

Significant Accomplishments and Conclusions:

Table 8: Final results

Key Metric		DOE 2030 Target	Status as of June 2025
Motor + Motor Controller Efficiency	**100% Flow**	92%	93%
	50% Flow	92%	94%
	Idle	80%	83%
Compressor/Expander Efficiency	**100% Flow**	75/70 %	66 / 62%
	50% Flow	80/80 %	70 / 57%
	Idle	62/60 %	63 / 0%
System Response Time		2 seconds	0.62 seconds
Durability		25,000 hours	Air system reliability 52% at 25,000 hours
Reliability		50,000 MBRC	Air system MBRC estimate 1.84M
Number of Startup Shutdown Cycles		50,000	See discussion in Task 2.
Noise at Idle		65 dB-A @ 1m	Between 63.6 and 67.2 dB-A.
System Cost		$3600	$3183
System Volume		0.25 L/kW	0.24 L/kW
System Weight		0.5 kg/kW	0.16 kg/kW
Turndown Ratio		20	43.2
System Efficiency Expressed as Air System Electrical Power Consumption for 300kW Fuel Cell:			
Electrical Power Consumption	**100% Flow**	27.9 kW	37 kW
	50% Flow	10.8 kW	9 kW
	Idle	0.32 kW	0.22 kW

The integrated compressor-expander developed in this project shows strong potential to reduce parasitic power in fuel cell air systems. Initial simulations predicted a ~50% reduction (24 kW), while final results showed ~24%. With insights from physical testing, Eaton believes the 50% target is achievable.

System response and stability were excellent, with a demonstrated turndown ratio of 43.2. Unlike centrifugal compressors, superchargers avoid surge issues, enabling safer low-flow operation. Durability, cost, size, and weight met or exceeded DOE targets.

While idle noise met expectations, Eaton anticipates noise concerns at 50% and 100% load in production systems. Though outside this project's scope, noise mitigation (e.g., baffling, resonators) will likely be needed at 50% and 100% load.

Path Forward:

Immediately following project, Eaton will be conducting tests on a new expander rotor design concept. New design concept is targeting isentropic efficiencies of ~80%. New rotor design aims to capture the air's kinetic energy by imparting a strategic leak to increase air speed and improve the pressure gradient across the rotor lobe. Testing planned to be completed in August of 2025.

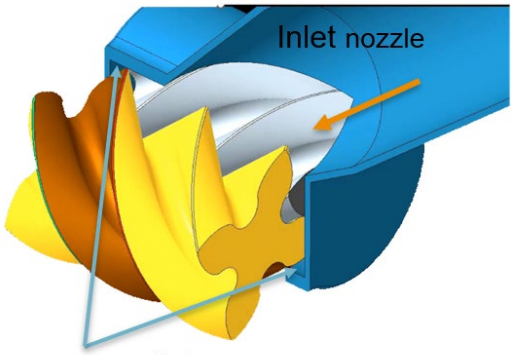

Figure 51: New expander rotor design

Products:

Journal Papers:

"High Efficiency and Transient Air Systems for Affordable Load-Following Heavy-Duty Truck Fuel Cells," Evan Reich, Matt Swartzlander, Jonathan Wine, James McCarthy, Jr., Saad Akhtar, Eric Miller, Sharan Reddy and TJ Lawy, Journal TBD, to be submitted for peer review in Aug 2025

"Comparative Analysis of Recuperator Integration in PEM Fuel Cell Air Systems, "Rakibul Hassan, Evan M. Reich, Brian Costello, James McCarthy, Jr and Riley B. Barta, Energy Conversion and Management, to be submitted for peer review in July/Aug 2025

"Numerical and Experimental Investigation of a Novel Fuel-Cell Air-Handling System for Medium-Duty/Heavy-Duty Applications," Saad Akhtar, Eric Miller, Jason Lustbader, Evan Reich, James McCarthy, Jr., Sharan Reddy and Thomas J. Lawy, Applied energy, to be submitted for peer review in July 2025

Patents / IP:

Patent/Application #	EIR #	Invention Title	Inventor(s)	Short Summary of Invention
63/583878	S-180,195	Low-Power Water Management for Fuel Cell Air Systems	Douglas Hughes	Low power consumption liquid water dosing methods for Fuel cell air handling system
	S-180,842	Fuel Cell Air System Architecture: Water Dosing Without Recuperator	Douglas Hughes, Evan Reich, Alexander W. Pomaville, Matthew Swartzlander	Fuel cell air handling system architectures with water dosing and energy recovery expander
	S-180,225	Recuperator and Intercooler Bypass for Fuel Cell Air System	Douglas Hughes	Addition of a bypass valve across recuperator and intercooler in Fuel cell air handling loop
	S-180,841	Fuel Cell Air System Architecture: Recuperator with Humidifier	Douglas Hughes, Alexander W. Pomaville, Evan Reich, Matthew Swartzlander	Fuel cell air handling system architectures with waste heat recuperator and membrane humidifier
-	-	Fuel Cell Air Recirculation for Humidity and Temperature Control	NREL will report through the M&O contract	Fuel cell air handling system architecture that recirculates air from the fuel cell outlet for humidification at the inlet
PCT/IB2024/063229	S-179,645	Gear type Air compressor with integrated water injection	Matthew Swartzlander	Method of introducing liquid water into positive displacement compressor for humidity control of fuel cell air handling systems
	10048558-24-0003	Roots Compressor Liquid Water Dosing Delivery Method	Evan Reich	Improved method for dosing liquid water into TVS compressor for humidity control in PEM fuel cell
	S-189,832	Closed Air Stream Liquid Water Sensing with Thermocouples	Evan Reich	Measurement strategy for detecting liquid water presence in fuel cell air system with an array of thermocouples
	S-190,229	Closed Air Stream Liquid Water Sensing with Thermocouples - update	Evan Reich	Improved measurement strategy for detecting liquid water presence in fuel cell air system with an array of thermocouples
	S-182,354	Incorporation of thin film evaporation within a positive displacement compressor	Matthew Swartzlander	Liquid water delivery method that encourages thin film evaporation in a positive displacement compressor for humidity control of fuel cell air handling systems
	S-179,657	Water injection to the low-pressure side of the compressor on a fuel cell using water collected in high pressure water traps at the inlet and outlet of the stack	Matthew Swartzlander	Method of liquid water dosing in fuel cell air handling system that uses the pressure differential across the fuel cell stack to push liquid water at the outlet of the fuel cell stack into the inlet of the compressor
	10048558-24-0004	Fuel Cell Cathode Air Water Dosing Temperature and Humidity Management Strategy	Evan Reich, Matthew Swartzlander	Strategy to use liquid water dosing to cool and partially humidify compressed air in fuel cell air handling system. Membrane humidifier performs the remaining humidification
N/A	S-180,171	Variable Displacement Expander using Water Dosing	Evan Reich	Adjust the effective displacement of a positive displacement expander by injecting a variable flow of liquid water into the expander
PCT/IB2024/058150	S-181,473	Anti-reverse rotation device applied for initial fuel cell startup	Matthew Swartzlander	For fuel cell air system architectures that utilize differential gearing between compressor and expander. One way clutch fitted between gearbox output and expander input shaft to prevent expander from spinning in opposite direction during air system startup
	10048558-22-0005	Fuel Cell Air System Architectures	Alexander W. Pomaville, Matthew Swartzlander, Douglas Hughes, Evan Reich	Various fuel cell air handling system architectures for improved power consumption
N/A	10048558-24-0005	Roots Compressor Liquid Water Dosing Freezing Mitigation Strategies	Evan Reich, Douglas Hughes, Matthew Swartzlander	Various strategies to prevent liquid water freezing from stopping functionality of water dosing system

Project Team and Roles:

Organization	Name	Job Title	Role in Project
~~Eaton~~	~~Doug Hughes~~	~~Chief Engineer~~	~~Principal Investigator~~
Eaton	James McCarthy	Chief Engineer	Principal Investigator

Eaton	Jonathan Wine	Engineer	Engineer
~~Eaton~~	~~Alex Pomaville~~	~~Senior Engineer~~	~~Controls Engineer~~
Eaton	Evan Reich	Senior Engineer	Mechanical Engineer
Eaton	Matt Swartzlander	Specialist Engineer	Mechanical Engineer
Eaton	Jeff Camilleri	Senior Technologist	Laboratory Technician
Eaton	Carlos Wink	Chief/Principal Engineer	Gear Engineer
Eaton	Gerald Burke	Senior Specialist Engineer	FEA Analyst
Eaton	Jim Spring	Lead Technologist	Designer
Eaton	Timothy Caudill	Senior Technologist	Metrology and Inspection
Eaton	Brent Rehm	Senior Technologist	Machinist
Eaton	Andrew Brubaker	Senior Technologist	Machinist
Eaton	Chris Frank	Senior Technologist	Designer
Eaton	Adithya Baburaj	Engineer	Controls Engineer
Eaton	Savan Adeshra	Engineer	Controls Engineer
Eaton	Michael Patton	Program Manager	Program Manager
~~Eaton~~	~~Adaeze Okorie~~	~~Program Manager~~	~~Program Manager~~
Ballard	TJ Lawy	Program Director, Balance of Plant Components	Ballard Technical Lead and Manager
Ballard	Sharan Reddy	Engineer	System Engineer
NREL	Eric Miller	Engineer	Modeling and Simulation Engineer
NREL	Jason Lustbader	Advanced Vehicles & Charging Infrastructure Group Manager	NREL Technical Lead and Manager
NREL	Sarah Wassigner	Administrative Assistant	Administrative Assistant
NREL	Saad Akhtar	Engineer	Modeling and Simulation Engineer
NREL	Chad Baker	Engineer	Modeling and Simulation Engineer
NREL	Matt Allen	Engineer	Hydrogen Production, Power, and Storage
NREL	Shaun Onorato	Engineer	Hydrogen Production, Power, and Storage
NREL	Katie Hurst	Group Manger	Hydrogen Production, Power, and Storage
NREL	Keith Wipke	Program Manger	Fuel Cell and Hydrogen Technology
NREL	Ken Kelly	Chief Engineer	Commercial Vehicle Technology

References:

NREL DriveCAT - Chassis Dynamometer Drive Cycles. 2023. National Renewable Energy Laboratory. www.nrel.gov/transportation/drive-cycle-tool

Roots Air Management System with Integrated Expander – DE-EE0005665. 2016. Eaton Stretch D., Eybergen W. https://www.osti.gov/servlets/purl/1325976

Seetharaman S and Kahraman A. A windage power loss model for spur gear pairs. Tribol Trans 2010; 53: 473–484

Concli, F. and Gorla, C., 2016, “Windage, churning and pocketing power losses of gears: different modeling approaches for different goals,” *Forschung im Ingenieurwesen/Engineering Research* **80**(3-4), pp. 85-99.

Diab, Y., Ville, F., Velex, P., and Changenet, C., 2004, “Windage Losses in High-Speed Gears. Preliminary Experimental and Theoretical Results,” ASME J. Mech. Des., **126**_5_, pp. 903–908.

Dawson, P. H., 1984, “Windage Loss in Larger High-Speed Gears,” Proc. Inst. Mech. Eng., Part A, Power and Process Engineering, 198_1_ pp. 51–59.

ISO 14179-2:2001, *Gears – Thermal capacity – Part 2: Thermal load-carrying capacity*.

A. Lord, (1998) An experimental investigation of geometric and oil flow effects on gear windage

and meshing losses, Ph.D. thesis, University of Wales, Swansea